CHALMERS
UNIVERSITY OF TECHNOLOGY

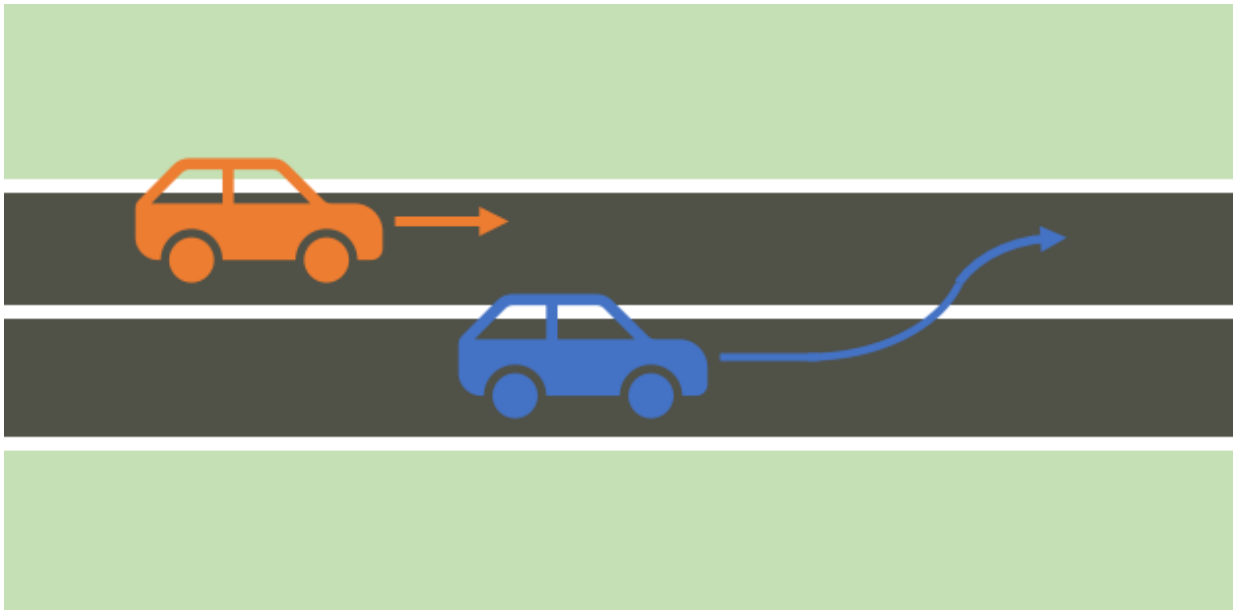

Driver Modelling for Virtual Safety Assessment of Automated Vehicle Functionality in Cut-in Scenarios

Accumulation Model Development Using SHRP2 Data

Master's thesis in Automotive Engineering

CHRISTOFFER CHAU
QIANYU LIU

DEPARTMENT OF MECHANICS AND MARITIME SCIENCE
CHALMERS UNIVERSITY OF TECHNOLOGY

Gothenburg, Sweden 2021
www.chalmers.se

MASTER'S THESIS IN PROGRAMME NAME

Driver modelling for safety assessment of automated vehicle functionality in cut-in scenarios

Christoffer Chau
Qianyu Liu

Department of Mechanics and Maritime Sciences
Division of vehicle safety
CHALMERS UNIVERSITY OF TECHNOLOGY
Göteborg, Sweden 2021

Driver modelling for virtual safety assessment of automated vehicle functionality in cut-in scenarios

Christoffer Chau
Qianyu Liu

Supervisor: Jonas Bärgman, Mechanics and Maritime Sciences
Examiner: Jonas Bärgman, Mechanics and Maritime Sciences

Master's Thesis 2021:55
Department of Mechanics and Maritime Sciences
Division of vehicle safety
Chalmers University of Technology
SE-412 96 Göteborg
Sweden
Telephone: + 46 (0)31-772 1000

Cover:
Graphical representation of cut-in scenario: a vehicle (blue) from adjacent lane is cutting in the front of the orange vehicle. The driver model developed in this thesis aims to predict the braking response of the vehicle (orange) being cut-in. Detailed descriptions of the cut-in scenario can be found in Section 1.2 and 2.1.

Department of Mechanics and Maritime Sciences
Göteborg, Sweden 2021-07-08

Driver modelling for virtual safety assessment of automated vehicle functionality in cut-in scenarios

Christoffer Chau
Qianyu Liu

Department of Mechanics and Maritime Sciences
Division of Vehicle Safety
Unit of Crash Analysis and Prevention
Chalmers University of Technology

Abstract

The development of active safety systems and automated vehicles has increased exponentially in recent years and can influence traffic safety in various ways. Prospective assessments of their safety impacts are required during the development of active safety systems and automated vehicle functionality. Virtual simulation is one of the most common approaches of safety prospective assessments; a method that uses models to represent drivers, vehicles and road environments, etc., and run simulations in computers to estimate the risk and benefit of safety systems. This thesis aims to extend and implement an existing rear-end accumulation driver model into a cut-in driver model in the virtual simulation tool Esmini. The model is for predicting the braking behaviour of the driver of a vehicle (going straight, denoted EGO vehicle) when another vehicle (denoted Principle Other Vehicle; POV) from an adjacent lane is cutting in in the front of the EGO vehicle. The model parameters were optimized to cut-in near-crashes from a set of Naturalistic Driving Data from The Second Strategic Highway Research Program (SHRP2) in the US. The stochastic machine learning method Particle Swarm Optimization was used to fit the braking onset timing and jerk, which represent the time when a driver starts to decelerate harshly and the ramp-up of the deceleration, respectively, as defined by a piecewise linear model of the behaviour observed in the SHRP2 data. Three different models were introduced and implemented in the virtual simulation framework. The performance of the models were good for some events, but could not capture the variability across all events sufficiently for direct use in safety assessment. Future work could include fitting the model to more data, as well as fixing some parameters to reduce the complexity of the current model and capturing more information, which could affect the driver response in a cut-in scenario. With further developments of the models, it may be used for safety assessment of active safety or other vehicle automation functions.

Key words: Driver model, Cut-in scenario, SHRP2, Naturalistic Driving Data, Automated vehicle, Particle swarm optimization, Virtual simulation, Active safety

Contents

Preface

This research is a master thesis work carried out at the Department of Mechanics and Maritime Sciences, Division of Vehicle Safety, Chalmers University of Technology, Sweden. The work was developed from January to August 2021, and part of the work was performed at the offices of the Vehicle and Traffic Safety Centre at Chalmers – SAFER, Gothenburg.

Acknowledgements

First, we would like to thank our examiner and supervisor Jonas Bärgman for his tremendous support throughout the thesis. Without your support, we don't think we would have made it this far. Not only did you support us with the research but also giving us advice for the future and we are extremely grateful for that. A special thanks to Giulio Bianchi Piccinini and Marco Dozza for your feedback during mid-presentation. In addition, we would like thank Xiaomi and Pierluigi for your advices and support on our research work. We would also like to thank SAFER for offering us a nice work environment.

We want to thank VTTI for sharing SHRP2 data with us in this research and permission for showing pictures in the report and presentation. We also want to thank esmini team for providing a free and open source simulation tool. A special thanks to Emil Knabe of his assistance in resolving Esmini-related issues. We would like to thank Riyam Tayeh, Ahmed Shams El Din, and Vignesh Krishnan from Volvo Cars for providing us the code to run Esmini.

We wish to thank all our friends, the ones we met in Sweden from all over the world and also our old friends, who are always be supportive during hard times. A special thanks to Kishore for all the discussions about related topics during coffee breaks. Last but not least, we would like to thank all our families who have supported us throughout our studies and been believing in us all the time.

This work has been performed under the VTTI SHRP2 Data License Agreement. The findings and conclusions of this report are those of the author(s) and do not necessarily represent the views of VTTI, the Transportation Research Board, or the National Academies. The data used falls within the licence agreement SHRP2-DUL-A-16-204 and the data has the DOI:10.15787/VTT1K013.

Göteborg March 2021-07-08

Christoffer Chau & Qianyu Liu

Notations

AS	Activity Safety
GUI	Graphical User Interface
POV	Principle Other Vehicle – the vehicle which the EGO vehicle is in conflict
EGO	The vehicle with the driver model, also known as the subject vehicle
SHRP2	Second Strategic Highway Research Program
NDD	Naturalistic Driving Data
VAT	Video Annotation Tool
PSO	Particle Swarm Optimization
GA	Genetic Algorithm
ADAS	Advance Driving Assistance System
AD	Automated Driving
VTTI	Virginia Tech Transportation Institute
FOT	Field Operational Test
DAS	Data Acquisition System
Euro NCAP	European New Car Assessment Programme
TTC	Time To Collision
Before POV-in-lane	The condition that the POV is completely outside the EGO vehicle's lane (has not crossed the lane marking)
After POV-in-lane	The condition that the POV is overlapping with the EGO vehicle's lane lane-marking, or the POV being inside the same lane as EGO vehicle
AIC	Akaike Information Criterion
t_B	Break onset timing - time when the driver started to break harshly
j_B	Jerk - ramp up of the acceleration

1 Introduction

In 2019 there were approximately 1.35 million fatalities and between 20 and 50 million people suffered non-fatal injuries (WHO 2020). As a result, road traffic accidents put a huge strain on all nations, both from an economic and social perspective (Markkula, 2014). Humans are the main reason why accident occur in the first place, and much research has been conducted to understand human behaviour in traffic and how to improve safety or avoid accident (Markkula et al., 2012). New active safety systems, advanced driving assistance systems (ADAS) and automated driving (AD) functionality have been developed to reduce the number and severity of accidents, and to help human drivers avoiding dangerous situation. These ADASs and ADs will help drivers to avoid or mitigate crashes by partially taking over the vehicle when the driver loses control, or they may send warning signals to alert the driver of imminent threats. The development of safety-relevant functions necessitates a quantitative assessment of their impact on traffic safety, taking into account both positive and negative aspects (Helmer et al., 2015). There are two types of assessment approaches: prospective assessment and retrospective assessment. The goal of retrospective assessment is to quantify the benefits or risks introduced by an ADAS or AD function after it has been in use in market for a period. Prospective assessment, on the other hand, is aimed to predict the effectiveness and expected safety benefits of a new functions.

Field Operational Tests (FOT), test tracks, driving simulators, accident analysis, and virtual simulations are the most commonly used prospective safety assessment approaches (Page et al., 2015). In FOT, the ADAS or AD functions are installed on vehicles and tested in real-world traffic. Because it involves normal drivers and real-world traffic situations, the FOT approach can produce robust and comprehensive results. However, it necessitates a significant amount of resources and comes at a high cost. In the test track approach, the functions are installed in a vehicle and tested in a test track with professional drivers under known conditions. In comparison to FOT, test track can test the functions under critical but controlled situation, avoiding putting drivers in danger. Because not all conditions can be tested on a test track and the drivers are professionals, the evaluation results are less reliable than FOT. It is very difficult, or, often, impossible, to extrapolate test track testing to actual safety benefits. Driving simulators can capture real driver's reactions in virtual simulations and enable repeated testing of new functions. But the fidelity is even lower than test track tests because drivers may react differently in virtual simulation and in real world. Virtual simulations, on the other hand, use computers to mimic (simulate) driving, which enable safety assessments in different scenarios at a reasonable cost, and depending on the data used as a basis, allows for actual estimates of absolute benefits of the safety system under assessment. However, using virtual simulation puts high requirements on driver models to guarantee accuracy and precision in the simulation results (Page et al., 2015).

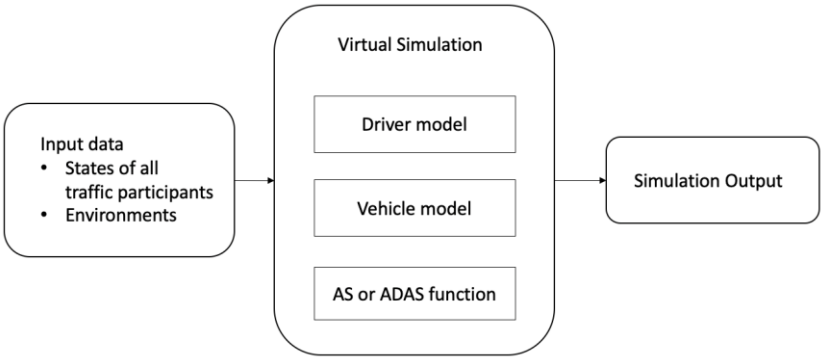

Figure 1 Virtual simulation

Scenario-based virtual assessment is one specific form of virtual simulations, used to quantify the effectiveness of a function in a specific scenario using simulations. The overall safety effectiveness is then calculated as the sum of effectiveness of all scenarios weighted by the frequency of each scenario (Helmer et al., 2015). A simple framework of virtual simulations is shown in Figure 1. Once the scenario is determined, the input dataset, which includes a collection of events from critical situations within the context of the specific scenario, is prepared for virtual simulations. The input dataset can either be synthetic data generated from the distribution of pre-crash conditions, or reconstructed from real-world driving data, such as Naturalistic driving data (NDD). The second Strategic Highway Research (SHRP2) naturalistic driving study is the largest naturalistic driving study program to date, having captured data about 3,400+ drivers and vehicles during their daily driving, including 36,000 crash and near-crash events. The Virginia Tech Transportation Institute (VTTI) was the technical coordination and study design contractor for the SHRP2 naturalistic driving study. The SHRP2 NDD provides detailed pre-crash, driver behaviours and exposure information, which can be used for research and develop different safety systems (Gordon & Srinivasan, 2014). The Data Acquisition System (DAS) used to collect the SHRP2 data contained a forward radar, four video cameras (including forward view, rear and right view, driver and left side view and passenger snapshot view), accelerometers (measuring the acceleration in the longitudinal, lateral and vertical direction), Geographic Positioning System (GPS), as well as gyroscopes measures (yaw rate, roll rate and pitch rate) (Virginia Tech Transportation Institute, 2020). To date there are more than 300 publications that utilize SHRP2 data in one way or another.

The input data generation for use of, for example, SHRP2 data, requires processing of raw NDD data. The Data Reduction Group from VTTI reduce the raw data into a format that allows specific research and have developed software tools to analyse eyeglance and other video-based data (Virginia Tech Transportation Institute, 2021). Further, an annotation tool was developed in previous work at Chalmers (Din et al., 2020) – a tool that can extract the distance to lane markings and other vehicles, by manually (semi-automatically) annotating the forward view video from SHRP2 events. The goal of developing the tool was to support manual annotation of NDD to extract the necessary data, such as lane markings, position and movement of the Principe Other Vehicle (POV; the vehicle with which the instrumented vehicle, called EGO vehicle, is primarily in conflict), for research.

As mentioned earlier, FOTs can be expensive when testing safety systems. Virtual simulation is a much more cost efficient and safe way of testing safety systems (Benderius, 2012). However, in virtual simulation, models are needed to represent drivers, vehicles, etc. Such models can be classified into two types: deterministic and stochastic. The output of deterministic models is fixed given a specific input and parameter set, whereas stochastic models produce randomness. There are many uncertainties in real world, for example different drivers may react differently in a critical situation and even the same driver may behave differently when exposed to the same critical situation. Hence, stochastic simulation should preferably be performed on large representative samples of virtual representations of crashes during the development and assessment of AS or ADAS functions. Further, computational models of drivers, vehicles, traffic flow, road environment and their interactions are required in virtual simulations as the representations of real traffic situations.

There are different driver models, such as driver control behaviour models in near-crash rear-end scenarios (Markkula, 2014) and models that keep a vehicle in the lane (Gordon & Srinivasan, 2014). Lee's (2012) research show how a driver might visually control his/her braking and how driver may control his/her braking and vehicle-following behaviour by monitoring the forward scene with the eyes (visually). Therefore, understanding how drivers visually gather information is important for improvement on road safety, as it is needed to develop accurate and realistic models of driver behaviour. Based on theory about visual cues an evidence-accumulation based driver model for car-to-car rear-end conflict was proposed by Svärd et al. (2017). The Svärd et al. model used perceptual visual looming to determine how "hard" the driver should brake to avoid collision. The model was further developed in Svärd et al. (2020). When developing models and fitting their parameters there is typically a need to have a framework to perform virtual simulations, so that some set of performance indicators can be compared between the model and the data it should be fitted to. Examples of such frameworks are Virtual Test Drive (Hexagon AB, 2021) and OpenPass (Invisiblefarm s.r.l., 2014). But also the open source simulation software Esmini (Emil Knabe, 2021) can be used as a basis for such a framework.

In this thesis, a driver model was developed for cut-in scenarios on highways, using data from the SHRP2 NDD as a basis. According to the European New Car Assessment Programme (Euro NCAP), a cut-in scenario is when a car from the adjacent lane merges into the lane in front of another vehicle (e.g., the vehicle which system is being assessed). Cut-ins happens in everyday driving, and a driver will usually anticipate the manoeuvre ahead of time and reduce speed accordingly. Chovan et al. (1994) report that there were approximately 244,000 lane change/merge crashes, that represented 4% of all crashes in the US, in 1991. In addition, Chovan et al. estimate that 386,000 non-police reported lane change/merge crashes happened in the US in the same year. As ADAS and AD functions are developed to handle cut-in events, it is increasingly urgent to develop models of driver behaviours in cut-in scenarios, for use in prospective virtual simulations to assess the systems impact on safety. (Shams El Din, 2020a). We have not found any scientific paper on driver modelling for cut-in scenario, however the rear-end accumulation driver model introduced in (Svärd et al., 2017) is related and could be used as the basis of developing driver model for cut-in scenario. The virtual simulation components required for driver model development are similar to those for safety assessment (as shown in Figure 1) but the AS and ADAS functions should be deactivated to ensure that the simulation outputs are independent of AS and ADAS functions interventions.

1.1 Accumulation driver model

An accumulation model of driver responses to critical situations in rear-end scenario was introduced in Svärd et al. (2017, 2020). The following is a brief overview of the Svärd et al. (2017) model (illustrated in Figure 2).

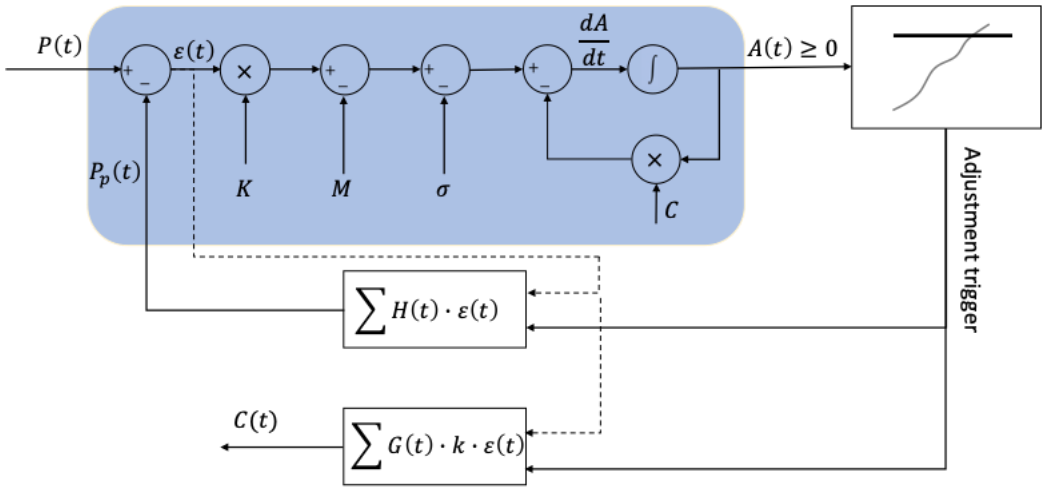

Figure 2 Accumulation driver model

In each timestep, the model collects perceptual evidence by noisy accumulation (as Equation (1) of the discrepancy between actual perceptual input $P(t)$ and prediction of it, denoted as $P_p(t)$.

$$\frac{dA(t)}{dt} = K * \mathcal{E}(t) - M - C \cdot A + v(t) \quad (1)$$

Where $\mathcal{E}(t)$ is the total perceptual error, and it can be calculated as:

$$\mathcal{E}(t) = P(t) - P_p(t) \quad (2)$$

where $A(t)$ is the accumulated evidence, called the activity, K, M and C are free model parameters (to be fitted to data). The details of each parameter can be found in (Svärd et al., 2020). $v(t)$ is the zero-mean Gaussian white noise with a standard deviation $\sigma\sqrt{\Delta t}$. Looming τ^{-1} (as Equation (3)) is inverse of time to collision (TTC) as described by variables that the human can perceive:

$$\tau^{-1} = \frac{\dot{\theta}}{\theta} \quad (3)$$

where θ is the optical size (horizontal angle) of the POV. The θ calculation for rear-end scenario can be seen Figure 3 and in Equation (4):

$$\theta = 2 \cdot \tan^{-1} \frac{W_{pov}/2}{d_x} \quad (4)$$

where W_{pov} is the width of the LV, dx is the longitudinal distance between the POV's rear bumper and EGO vehicle's front bumper.τ^{-1} was used as the models perceptual input in (Svärd et al., 2017).

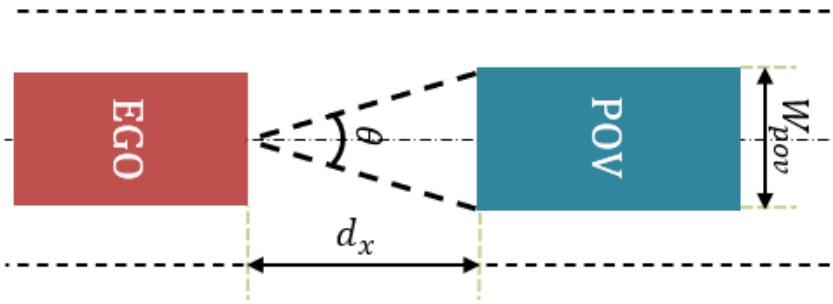

Figure 3 Optical size of POV in read-end scenario

Once the activity, A, exceed a pre-defined threshold, the driver model will issue a brake signal to the vehicle models brake actuation. The amplitude of the brake adjustment is determined by a linear function $G(t)$, as shown in Figure 4, scaled by the brake gain parameter k and prediction error $\varepsilon(t)$, which represents the braking increasing linearly to the target level within the adjustment duration $\triangle T$. After each brake adjustment, the activity A will be reset to a lower value A_r and prediction $P_p(t)$ will be updated to a scaled of prediction error with time-varying scaling factor $H(t)$, as shown in Figure 5. This is done for every timestep in the simulation.

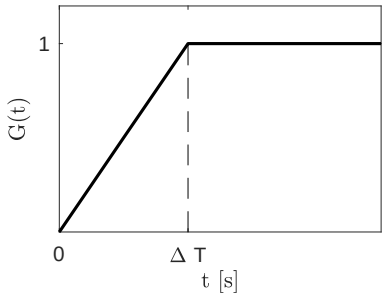

Figure 4 Plot of G(t)

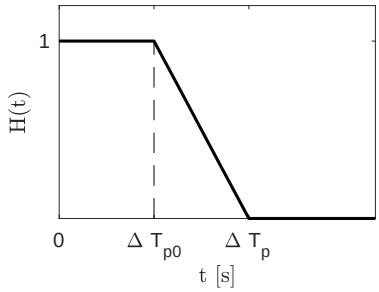

Figure 5 Plot of H(t)

There are eight free model parameters (K, M, C, σ, A_r, k, ΔT_{p0}, ΔT_{p1}) in total in the Svärd et al. (2017) model. After the 2017 publication, Svärd further developed the model. In (Svärd et al., 2020) some additional parameters were added (to also account for glances off road), and the model parameters were fitted to the SHRP2 data using Particle Swarm Optimization (PSO) – the break onset timing t_B and jerk j_B was the variables which were predicted (which the model should predict). The value of noise item ($v(t)$ in Equation 1) changed over time, resulting in non-deterministic responses from driver model. The simulation of each event in each PSO iteration was repeated 1000 times, and different acceleration output was obtained for each iteration. The driver model acceleration output from each simulation was fitted to a piecewise linear function to get the break onset timing t_B and jerk j_B. The t_B and j_B values obtained from repeating simulations were used to generate a 2D probability distribution. The SHRP2 acceleration values of event i were also fitted into the piecewise linear function to obtain the reference value ($t_{B,i,ref}$, $j_{B,i,ref}$). The $\ell\left(t_{B,i,ref}, j_{B,i,ref} \middle| \mathbb{P}_{j,k}\right)$, denotes likelihood of the reference value with given parameter set $\mathbb{P}_{j,k}$(parameter set of the j th

particle in the k th iteration), was estimated to calculate the fitness of the model. The cost function provided in Svärd et al., (2020) was then the total log likelihood of all events in training set using parameter set $\mathbb{P}_{j.k}$, with compensation of potential outlier as:

$$\log \mathcal{L}\left(\mathbb{P}_{j.k}\right) = \sum_{i=1}^{N} \log\left(\rho \cdot \ell\left(t_{B,i,ref}, j_{B,i,ref} \middle| \mathbb{P}_{j.k}\right) + (1-\rho) \cdot p_v\right) \quad (5)$$

Where p_v is the outlier compensation term, that was calculated as:

$$p_v = \frac{1}{t_{B,max} \cdot j_{B,max}} \quad (6)$$

With this method, the parameter set with the highest total log likelihood provides the best fit of SHRP2 training events.

1.2 Aim and objectives

The aim of this thesis was to develop a computational driver model of driver brake responses in critical situations where a vehicle (POV) in an adjacent lane cuts-in in front of the vehicle (EGO) going straight (with the driver model). To make this possible, understanding driver behaviour in traffic is necessary. To achieve that, a developed annotation tool from Din et al., (2020) was utilized to extract the vehicle kinematics from near-crashes from the SHRP2 NDD dataset. The extracted kinematics was used to reconstruct a set of cut-in events, so that they could be simulated in a simulation environment (Esmini). The driver braking model was applied to each reconstructed event, but with the brake response in the original event removed. Results of the model and the original events were then compared, and the parameters optimized to provide best overall model fit to the data across all events. The driver model development was based on previous work on accumulators as part of modelling human behaviour for rear-end conflicts (Svärd et al., (2017). The parameter fitting/training and simulation run was done in Python, with Esmini as simulation engine. The parameter optimization for the driver model was similar to that of the research by Svärd et al. (2020), where PSO was used. Specifically, the driver model developed in this thesis aims to predict the braking response of the vehicle being cut-in (i.e., the vehicle going straight), hereafter known as the EGO vehicle. Note that steering of the EGO vehicle was not covered in this thesis and only passenger car drivers' responses to cut-ins were included in this research. Figure 6 visualizes the cut-in scenario, in which the lead vehicle, referred to as POV, changes lanes and cuts in front of the following vehicle, referred to as the EGO vehicle. Based on the original rear-end accumulation model new strategies to calculate looming, additional functions to trigger/accumulate perceptual input related to distances or angles, were developed in this thesis, for the model to handle cut-ins (rather than only rear-ends).

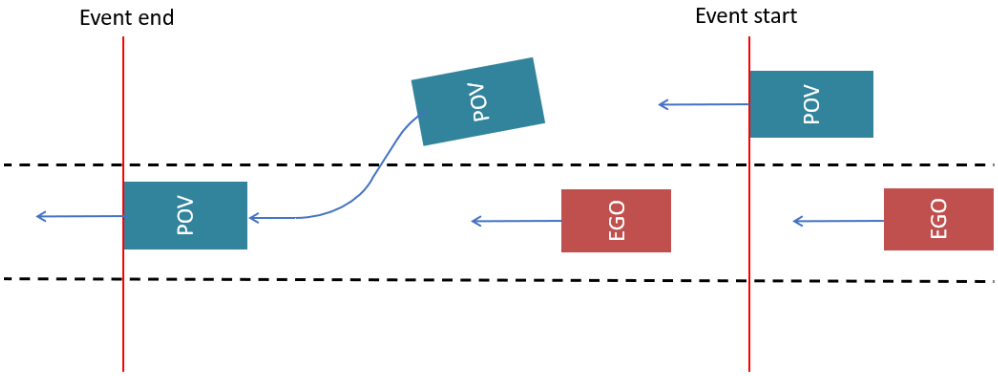

Figure 6 Event start and end in a cut-in scenario

To achieve the aim, several objectives needed to be fulfilled along the way. The detailed objectives were as follows:

- Extract and process the trajectory coordinate from SHRP2 data.
- Develop a cut-in driver model to predict the braking of EGO vehicle for the scenarios where the POV is entering the EGO vehicle lane from an adjacent lane, in front of EGO vehicle.
- Implement and further develop on current accumulation model for the cut-in driver model in Esmini.
- Train the cut-in driver model using the machine learning method particle swarm optimization (PSO) to fit the SHRP2 driver behaviour to the simulation output in terms of brake onset timing and jerk.
- Evaluate the cut-in driver model with respect to goodness of fit.
- Compare model approaches/parameterizations.

2 Methodology

The method used in this thesis will be explained in detail in this chapter. Figure 7 shows the work process of the implementation, parameterization, and parameter fitting of the driver model through virtual simulations, using data from the SHRP2 Naturalistic Driving Data (NDD) set. The evasive driver's behaviours were removed from SHRP2 data before fed into simulations. The vehicle and driver models were embedded in the virtual simulation tool Esmini (Emil Knabe, 2021). Volvo Cars provided a script in Python code to run Esmini for this research, therefore Esmini was chosen for this thesis. The accelerations from the driver model outputs were compared to the original SHRP2 acceleration in terms of break onset timing and jerk (a piecewise linear fit was done for both the model output and the original data). Section 2.1 and 2.2 describe how the trajectories of vehicles and coordinates of lane markings were extracted from the SHRP2 NDD. Section 2.3 explains how the rear-end accumulation driver model was modified to models for cut-in scenario in different ways. Section 2.4 shows the model parameter optimisation process.

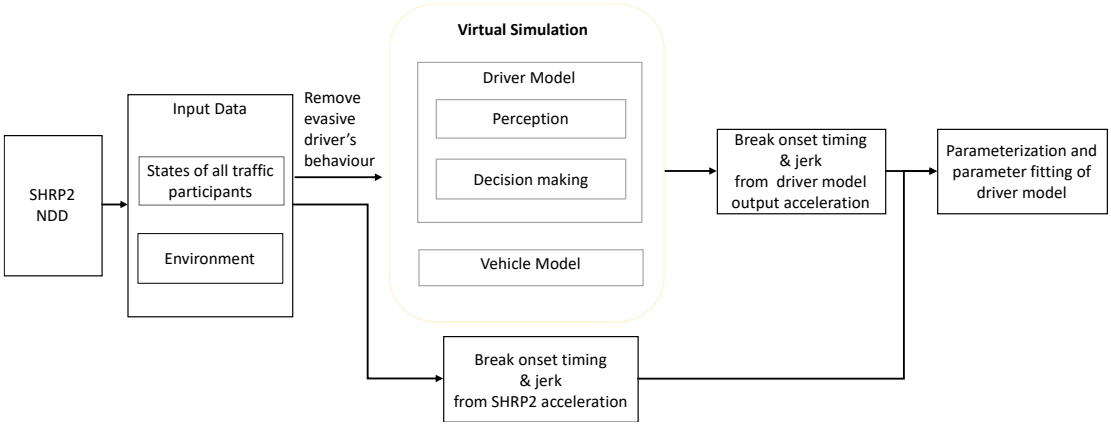

Figure 7 Driver model development

2.1 Events selection and annotation

To ensure that the driver model can represent real-world driver behaviour, it was tested and optimized using SHRP2 NDD. The forward facing video recordings from SHRP2 were manually annotated with an annotation tool developed during previous student work (Shams El Din, 2020b, Shams El Din, 2020b). Figure 8 shows the Graphical User Interface (GUI) of the annotation tool. The forward-facing video of the selected event can be played, with the annotator having the option of playing it at normal speed, fast speed, or frame by frame. By clicking points on a lane mark, the annotation tool can calculate the relative lateral distance between the lane mark and the EGO vehicle. The relative distances between POV and EGO vehicle in both longitudinal and lateral directions can be obtained by drawing a box on POV that covers the POV's rear lamps.

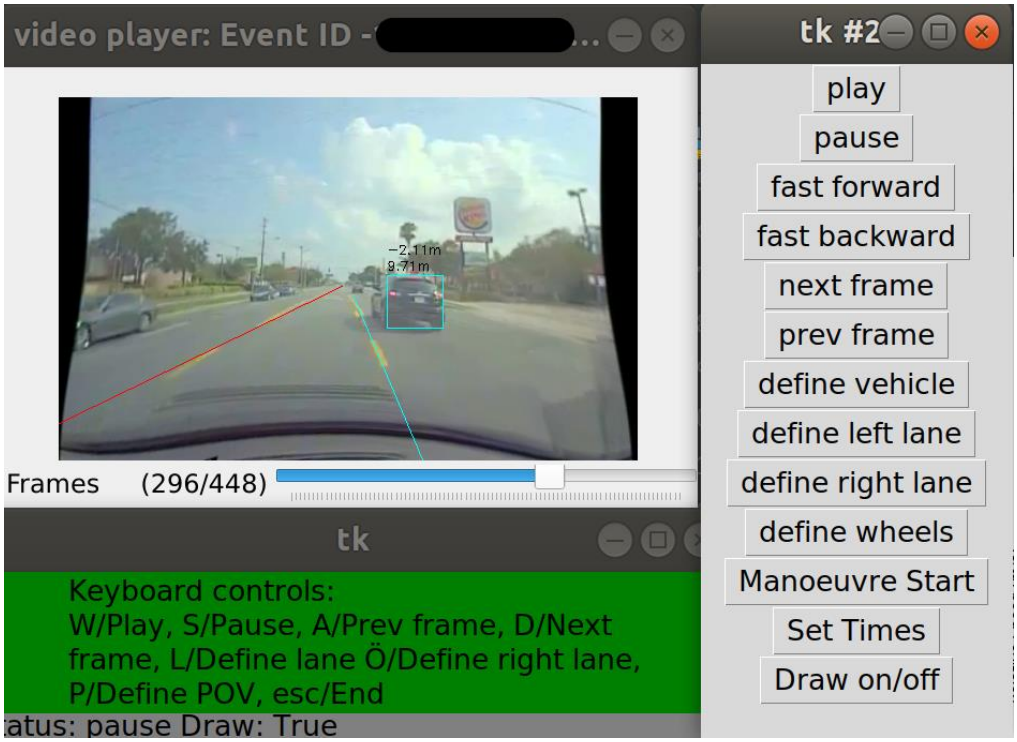

Figure 8 Annotation Tool GUI

Not all the events are suitable for annotation. The lane markings should be clear and the rear lamps of POV should be visible throughout the cutting-in process. Before annotation, the forward-facing videos of 209 cut-in events from SHRP2 were manually viewed to remove the events that were not suitable for annotation. Inclusion and exclusion criteria for annotation of events can be found in Table 1. Inclusion criteria represent all the necessary criteria that needed to be fulfilled (included in the event), while exclusion criteria represent possible factors or characteristics of an event that were excluded as they either were not needed in the modelling or made it difficult to make the events consistent. That is, events that did not fit the scenario which the model is sought to represent.

Table 1 Criteria for events selection

Inclusion criteria	Exclusion criteria
• Fully visible rear-lamp of POV before start of the event • Clear lane markings throughout the event • POV clearly visible throughout the event	• Non cut-in events • EGO steering • EGO changing lane • Lane merging or splitting

A visualization from a bird view perspective of non-cut-in events, EGO steering to avoid collision and EGO changing lane, can be seen in Figure 9.

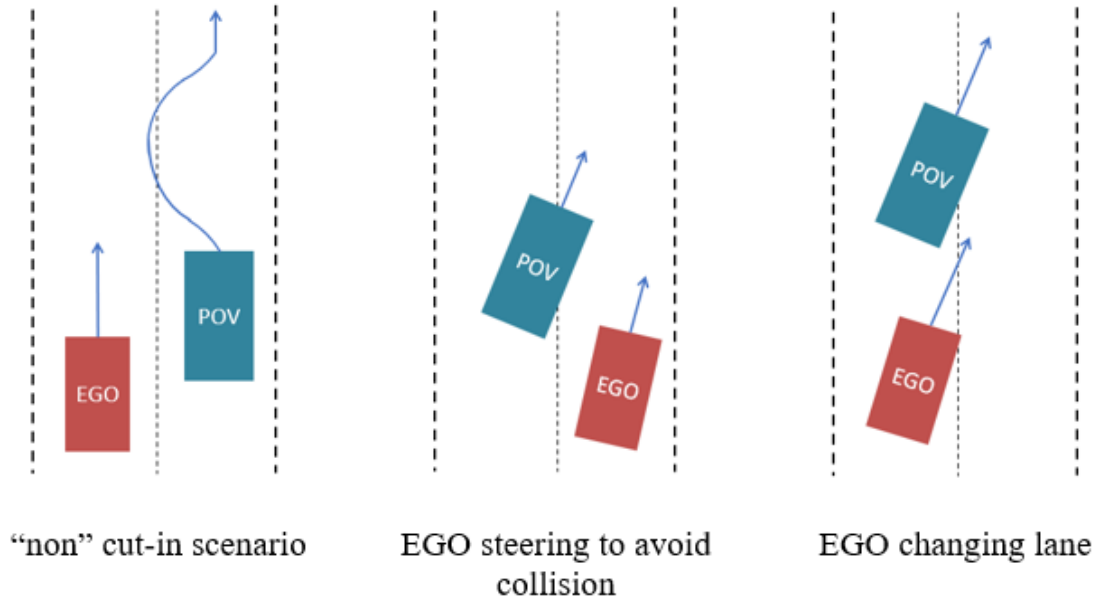

Figure 9 Demonstration of exclusion criteria

Lane marks have a very important role in the driver model in cut-in scenarios. The driver will respond differently depending on the position of the POV. The timing of when the POV is entering the EGO lane or touching the lane marking will impact the way the driver responds. A more detailed explanation of POV-in-lane is presented in the data-processing section. Since the lane marks have an important role, this can generate some potential problems when the lane marks are missing or not the same as real-world traffic (e.g., through issues in the annotation process) when generated in simulation. There were a couple of occasions where lane merging or lane splitting meant there were no lane marks, see Figure 10. In this event, the EGO lane is splitting into two different and the POV is cutting in from the right. The user (annotator) has to "assume" where the lane marks might be located and try to fill the missing gap and could potentially cause some mismatch between front view video and annotation output. Consequently, such events were removed.

Figure 10 Lane splitting

Missing data is inevitable and was bound to happened. There are events with no RADAR data and events with RADAR data, see Figure 11 (left upper and lower) for events with no RADAR data and Figure 11 (right upper and lower) events with RADAR data. Annotated data is marked with red dotted line (Figure 11 left upper and lower), while raw data (data from RADAR) is marked with normal lines with different colours (Figure 11 right upper and lower). Each colour describes the radar range from the ego vehicle to one (other) individual vehicle. Multiple colours indicate there are multiple vehicles in front of the EGO vehicle (can be in the ego vehicles lane, or in the adjacent lanes). This could be problematic if there are many vehicles in front and finding the correct vehicle will be hard. Luckily, this can be solved by finding which line is closest to the dotted line (annotated data) and then the user will know which is the correct vehicle. Another potential problem is the differences in longitudinal distance (longitudinal offset) between annotated data and RADAR data. This can cause a mismatch between simulation and the real event from SHRP2.

To find the longitudinal offset, only the top left and the top right figure (Range on the y axes) in Figure 11 are interesting. By not having any raw data, the annotators will have a hard time to compare if the annotation (box of the vehicle) is correct or not, with respect to the estimate of longitudinal distance to the POV. With RADAR data, annotators can compare the RADAR range and the range estimated from the annotation, and check if the result looks reasonable or not (see Figure 11, right picture). This information can later be used to eliminate any large offset from the real data in data processing (note that the RADAR typically only captured the vehicle late in the cut-in process, and not actually the lateral motion towards the lane).

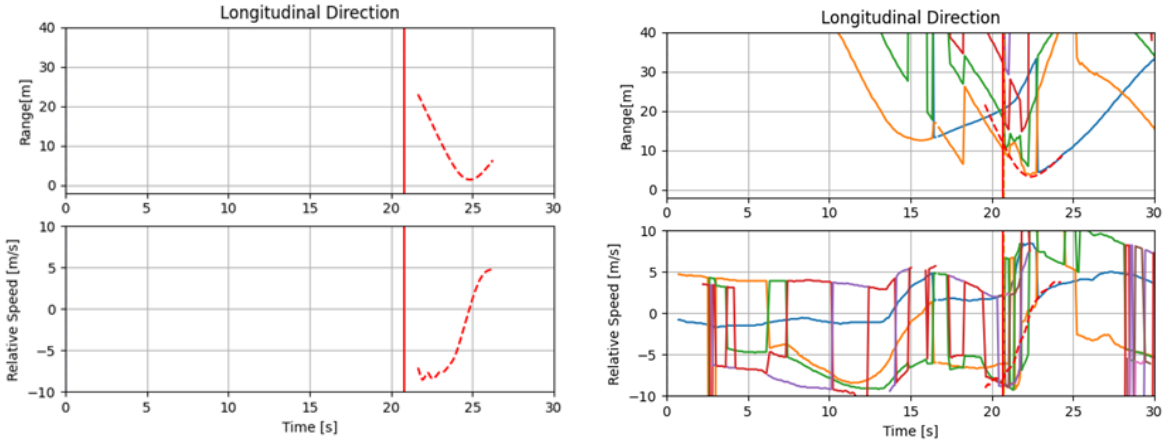

Figure 11 RADAR data example. The dashed line is the annotated data. Left X, right Y

Acceleration is another important piece needed for development of driver model. The data is crucial for acceleration fitting to find the reference value $t_{B,i,ref}$ and $j_{B,i,ref}$ from the model. A more detailed explanation can be found in section acceleration fitting (Section 2.1.1.1). By following the criteria presented in Table 1, remaining events were down to 51 and following the criteria presented in Table 1, only 18 events was selected out of 51.

2.2 Data processing

After selection of the events from SHRP2, the output from the annotation tool needed to be converted into another data format to be able to run the Esmini simulation. All coordinates, extracted from the annotation tool, were after annotation in the EGO vehicle coordinate system, denoted with superscript v. To enable usage of the data in Esmini simulations, the coordinates needed to be converted from the local (EGO vehicle) coordinate system into global coordinates, denoted with superscript g, as shown in Figure 12.

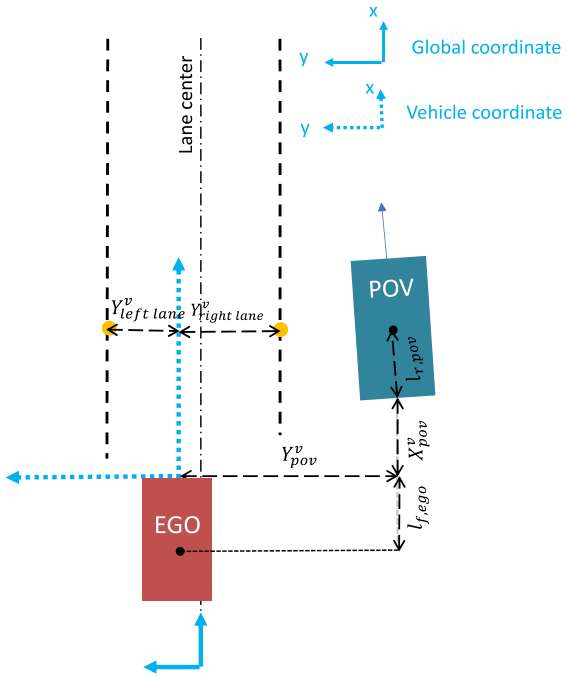

Figure 12 Coordinate conversion

In the longitudinal direction, the positions of the EGO vehicle were calculated by integrating the CAN speed from SHRP2 data as:

$$X^g_{EGO} = \int v_{x,EGO}\, dt \tag{7}$$

The x coordinates of POV and lane markings were then calculated as:

$$X^g_{POV} = X^g_{EGO} + X^v_{POV} + l_{f,EGO} + l_{r,POV} \tag{8}$$

$$X^g_{left\ lane} = X^g_{POV} \tag{9}$$

$$X^g_{right\ lane} = X^g_{POV} \tag{10}$$

In the lateral direction, the global coordinates can be obtained by assuming that the centre of the lane is straight:

$$Y^{g}_{lane\ center} = 0 \tag{11}$$

Hence, the y-coordinates of the left lane, right lane, EGO and POV, in global coordinate system, can be calculated as:

$$Y^{g}_{left\ lane} = Y^{v}_{left\ lane} - Y^{v}_{lane\ center} \tag{12}$$

$$Y^{g}_{right\ lane} = Y^{v}_{right\ lane} - Y^{v}_{lane\ center} \tag{13}$$

$$Y^{g}_{EGO} = Y^{v}_{EGO} - Y^{v}_{lane\ center} \tag{14}$$

$$Y^{g}_{POV} = Y^{v}_{POV} - Y^{v}_{lane\ center} \tag{15}$$

where $Y^{v}_{lane\ center}$ was calculated as:

$$Y^{v}_{lane\ center} = \frac{Y^{v}_{left\ lane} + Y^{v}_{right\ lane}}{2} \tag{16}$$

when the annotator is annotating, the annotation tool's output ranges that are constantly plotted together the RADAR range. If there is a large offset between the longitudinal range from the annotation tool and the RADAR, the annotator could remove the error it by changing the estimated hood length of EGO vehicle in the annotation tool, to ensure a good range estimating quality of the longitudinal range from the annotation tool (Shams El Din, 2020a). In this thesis, the lateral range is also critical. Because the driver model response was divided into two conditions: before the POV-in-lane and after POV-in-lane (details of the driver model response will be described in model part). Before POV-in-lane, as shown in Figure 13 (a), is when the POV is completely outside the EGO's lane, i.e., it is in other lanes and there is no overlap between the POV and the lane markings. While after POV-in-lane is when the POV is overlapping with the lane markings or the POV is inside the EGO's lane. Figure 13 (c) shows an example of after POV-in-lane. The time when the POV reached the lane marking, as shown in Figure 13 (b), is denoted as POV-in-lane timing.

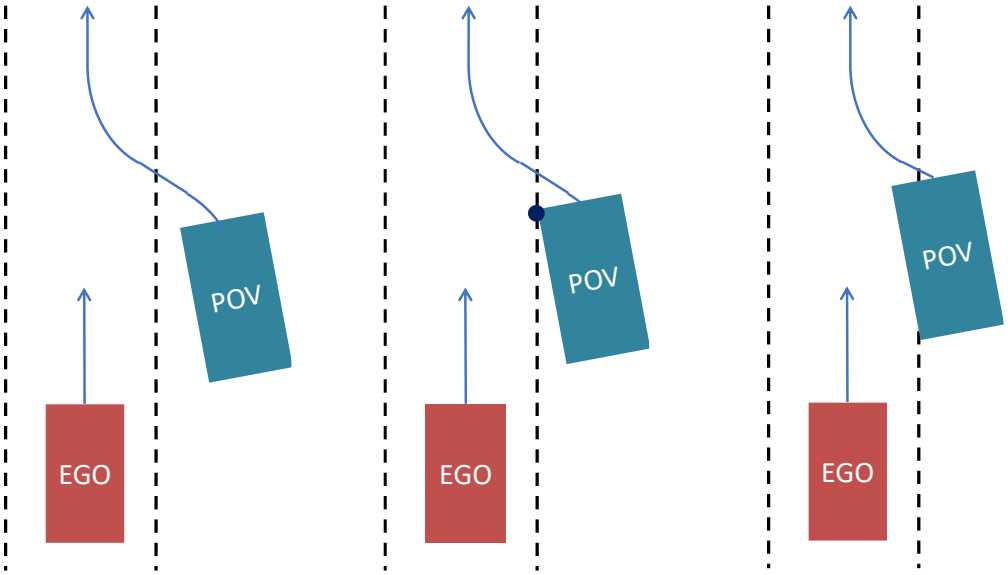

(a) Before POV-in-lane *(b) POV-in-lane timing* *(c) After POV-in-lane*

Figure 13 Before and after target-in-line

It is critical to ensure the data quality of the lateral range from POV to the lane marking and the POV-in-lane timing, as they have a substantial impact on the driver model response. There were clear differences between the annotation output and the front video for these two items. The errors were discovered in the late phase of this thesis. Consequently, manual modifications of the POV lateral positions were performed for each event due to project time constrains. The manual modification consisted of two steps, as shown in Figure 14 and Figure 15. Figure 14 is an exaggerated sketch while Figure 15 shows a real event example.

The first step was for fitting the real POV-in-lane timing. The video frame from SHRP2 when the POV reached the lane marking was noted down from visually checking the front view video, which is corresponding to the time step (denoted as t_1) when the actual lateral range between POV and lane marking was zero. The lateral distance between the POV and lane marking from annotation tool output at t_1 was calculated, denoted as error e_1, as shown in Figure 14. The POV lateral position was then shifted in the lateral direction so that the POV, in the top-view global coordinate view, entered the EGO vehicle lane at the same time. All the data points before $t_1$were shifted along the lateral direction with same amount of offset (e_1). The shifting amount decreased linearly from e_1 to zero from t_1 to three seconds later. We chose 3 seconds after trial-and-error as it provided a smooth trajectory across the datasets while not being a longer duration than what we had data for. In Figure 14, the longitudinal distance between t_1 and t_1+3s is much shorter than it is in real cases (to emphasise the lateral errors). Figure 15 shows a real (typical) case, with the offset gradually decreasing to zero after the POV enters into the same lane as the EGO vehicle.

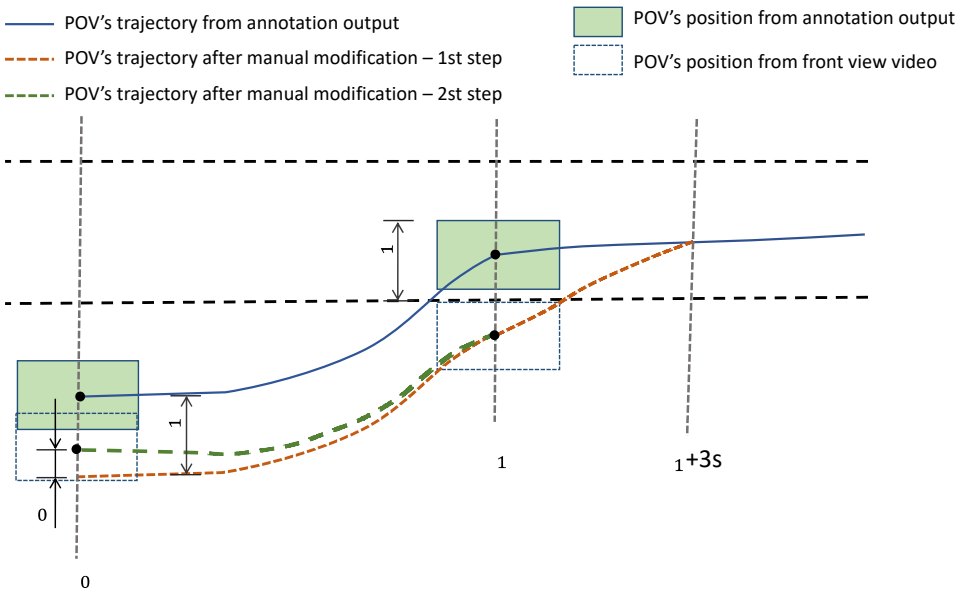

Figure 14 Much exaggerated manual modification process of POV trajectory

The e_1 was calculated assuming a zero-heading angle and the value of e_1 for each event was manually tuned to compensate for changes in POV-in-lane timing introduced by heading angles and trajectory smoothing in later data processing.

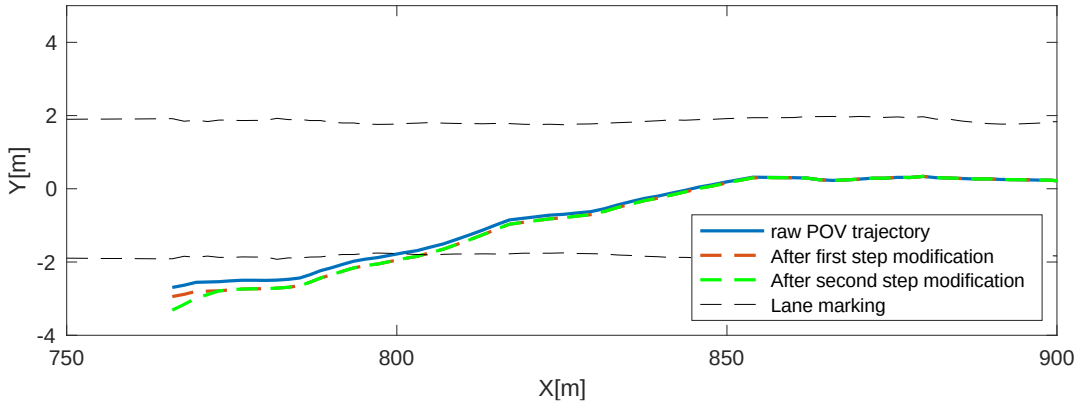

Figure 15 A real typical example of manual modification of lateral position of POV

In the second step, the lateral range between POV and the lane marking at first annotation time step (from which the data was available, denoted as t_0 in Figure 14) was visually inspected. The lateral range error at t_0 (denoted as e_0 in Figure 14) between the trajectory after the first step modification and visually inspection from front view video was calculated. The lateral range errors were removed by shifting the trajectory of POV laterally and the amount shifted decreased linearly from e_0 at t_0 to zero at t_1. That is, the top-view was compared to the video at the first frame of available data for each event, and the lateral position of the POV was modified until the top-view (in global coordinates) looked like what the position was in the forward video. After the two points (POV-in-lane and first frame in data) was established, all data points were shifted linearly across the entire dataset, so that the data passed through the two identified points.

The trajectory and lane coordinates in global coordinate were then smoothed by B-spline, converted into OpenDRIVE and openSCENARIO files, which are the data format for virtual simulation tool ESmini. The front view video and bird view plot of OpenDRIVE and OpenSCENARIO file for each event was played in the same window for final visual inspection of data quality. Figure 16 shows an example of screenshots of video of one event in three different time steps. The lateral range in bird view (reconstructed data) visually matches that in front view video, to verify that the events looked "the same".

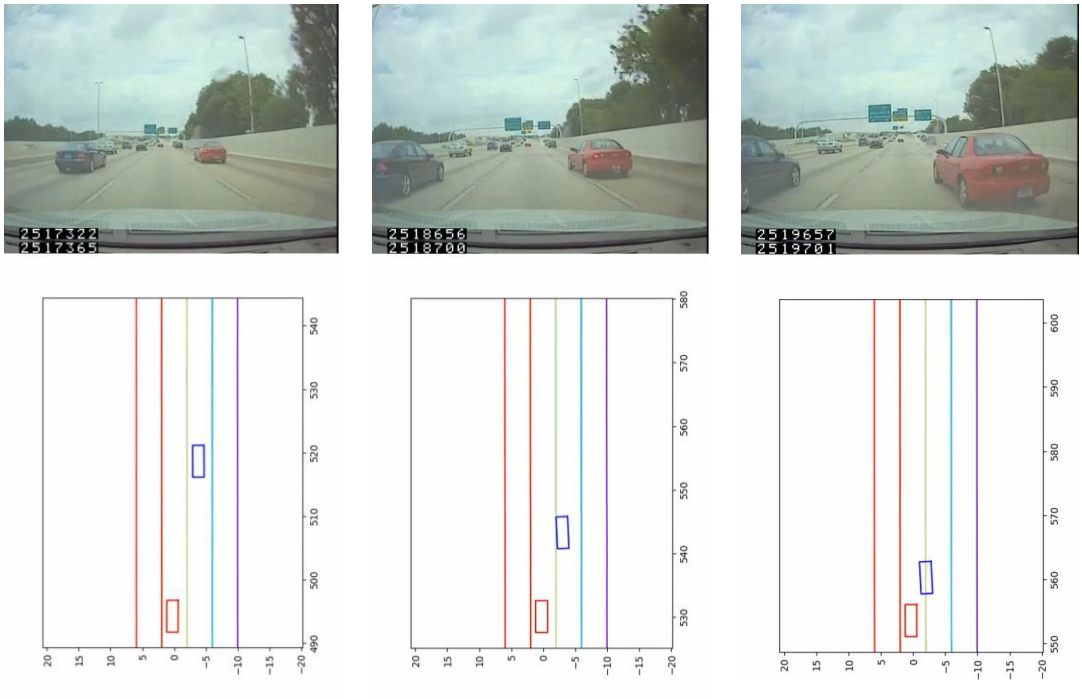

Figure 16 Example of a final visual inspection of data quality

2.3 Cut-in driver model

In the rear-end driver model by Svärt et al. (2017), the perceptual input $P(t)$, i.e., looming, can not be used directly in the cut-in scenario, as the lateral offset between EGO vehicle and POV also must be considered for this specific scenario. In this thesis work, the rear-end model was modified to be more "suitable" for cut-in scenarios, by changing the perceptual input $P(t)$. A couple of parameters were added to the "new" driver model for the cut-in scenario. Three proposals of modifications of the rear-end (Svärt et al., 2017) driver model, to make it relevant for use in the cut-in scenario, was proposed. All three related to how the $P(t)$ calculation is made. ΔT_{p0}, ΔT_{p1} were fixed to 1.5s for all models in this thesis, the values were from reduced-complexity models in Svärd et al., (2020). Two model parameters were fixed to simplify the parameter fitting, as it already was on the boarder that we would not be able to do the fitting (given the time it took to run all the simulations in the PSO fitting).

2.3.1 Model 1

In model 1, $P(t)$ was set to zero before POV-in-lane, i.e., the accumulation of looming error was only activated after POV-in-lane. However, it is unreasonable to have a zero $P(t)$ before POV-in-lane, because a human driver is unlikely to completely ignore all other road participants outside the lane in real world. Hence, Model 1 is an incomplete cut-in model, but it was used as a reference and as a basis for Model 2 and Model 3. The calculation of the optimal angle θ was also different from the rear-end driver model. Two different approaches on how to calculate θ was introduced in QUADRAE (2021). The first option was to use the angle of the rear bumper (AORB), and the second option was to use the angle of the full vehicle (AOFV). AORB was neglected because of potential problems when the POV is cutting into the lane at the very last moment or very close to the EGO vehicle. When the POV is cutting in very close to the EGO vehicle, the angle becomes smaller as it cuts in, and the activity level might decrease, see Figure 17. Therefore, the driver will, if only using looming, not be able to brake in time or not braking at, which will result in crash. That is consequently not a likely perceptual cue used by drivers to judge if a vehicle is about to cut-in. With AOFV, the angle does not become very small and activity level will be high. The driver will perform a braking manoeuvre (more) on time, compared to AORB, see Figure 17. Hence in Model 1 the perceptual input was calculated as Equation (17).

$$p(t) = \begin{cases} 0, & \text{before POV} - \text{in} - \text{lane} \\ \dfrac{\dot{\theta}_{FV}}{\theta_{FV}}, & \text{after POV} - \text{in} - \text{lane} \end{cases} \tag{17}$$

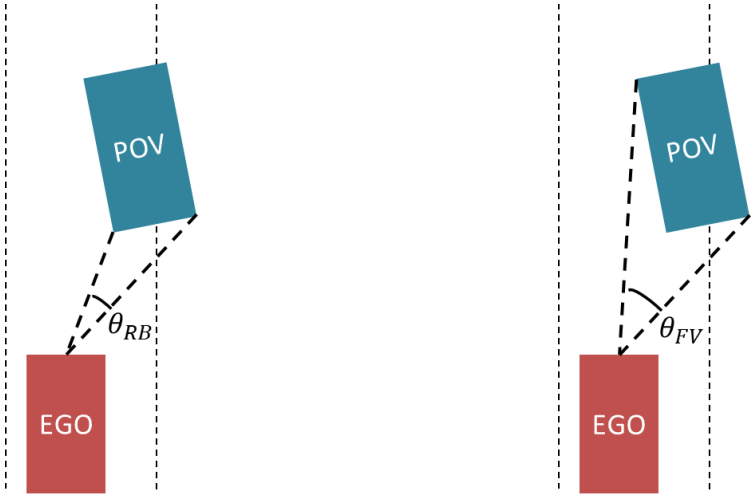

Figure 17 Rear bump angle and full vehicle angle

2.3.2 Model 2

In the real world, even if the POV does not yet reach the lane marking, the driver of the EGO vehicle will most likely begin to react after noticing that the POV intends to enter the lane, and thus often start braking already before it enters its lane (which Model 1 assumes). If the accumulation only begins after POV-in-lane, it is typically too late, especially when the POV is close to the EGO vehicle. In model 2, the algorithm was the same as Model 1 after POV-in-lane, which is accumulating looming error (of

AOFV). A new perceptual input was required to compute the evidence of braking before POV-in-lane. A linear scaling of inverse of time to cross lane was introduced and can be used as a "perceptual" input (not quite perceptual as in in terms of as it being based on perceptual variables that it has been shown that humans use, but a variable that eventually could be expressed as such – but that is out of scope of this thesis):

$$p(t) = \begin{cases} k_{pre} \cdot \dfrac{\dot{d}_{y,pov2lane}}{d_{y,pov2lane}}, & \text{before POV} - \text{in} - \text{lane} \\ \dfrac{\dot{\theta}_{FV}}{\theta_{FV}}, & \text{after POV} - \text{in} - \text{lane} \end{cases} \tag{18}$$

where $d_{y,pov2lane}$ is the lateral distance between the lane marking and the closest POV corner, as shown in Figure 18, and $\dot{d}_{y,pov2lane}$ is the time derivative of $d_{y,pov2lane}$. However, it can only represent how critical the situation is in the lateral direction, and it will go to infinity when the POV is approaching the lane, since $d_{y,pov2lane}$ is nearly zero, causing the perceptual error to go to infinity and the activity to reach the threshold quickly, even if the POV is very far away from EGO vehicle in the longitudinal direction. Considering only the lateral component would cause a braking signal to be issued, which often will not be in line with the data. Consequently, taking both the lateral and the longitudinal distances into account, the perceptual input was modified to:

$$p(t) = \begin{cases} k_{pre} \cdot \dfrac{\dot{d}_{y,pov2lane}}{d_{y,pov2lane} + k_{dx} \cdot d_x}, & \text{before POV} - \text{in} - \text{lane} \\ \dfrac{\dot{\theta}_{FV}}{\theta_{FV}}, & \text{after POV} - \text{in} - \text{lane} \end{cases} \tag{19}$$

where d_x is the longitudinal distance between the middle point of EGO vehcle's front bumper and POV's rear bumper, and k_{pre} and k_{dx} are two additional free model parameters. The perceptual error will be large with the modified perceptual input when POV is approaching lane marking and will not reach infinity. Moreover, a larger d_x, indicating the situation is less critical, will result in a smaller perceptual error and more slowly increasing activity.

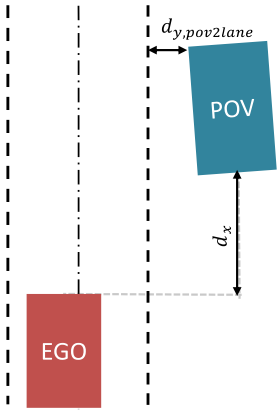

Figure 18 Distances

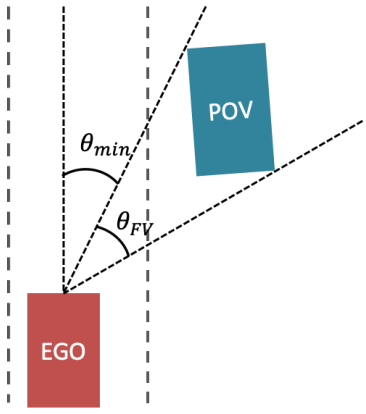

Figure 19 θ_{FV} & θ_{min}

2.3.3 Model 3:

The perceptual input after POV-in-lane for Model 3 is the same as Model 1 and Model 2. But before POV-in-lane, the perceptual input of model 3 is based on monitoring angels rather than distances. Two angles θ_{FV} and θ_{min}, as shown in Figure 19, were studied to determine perceptual input before POV reaching the lane marking. θ_{min} is the smallest of the angles between the longitudinal direction and the connecting line from the centre of EGO's front bumper to the corners of POV.

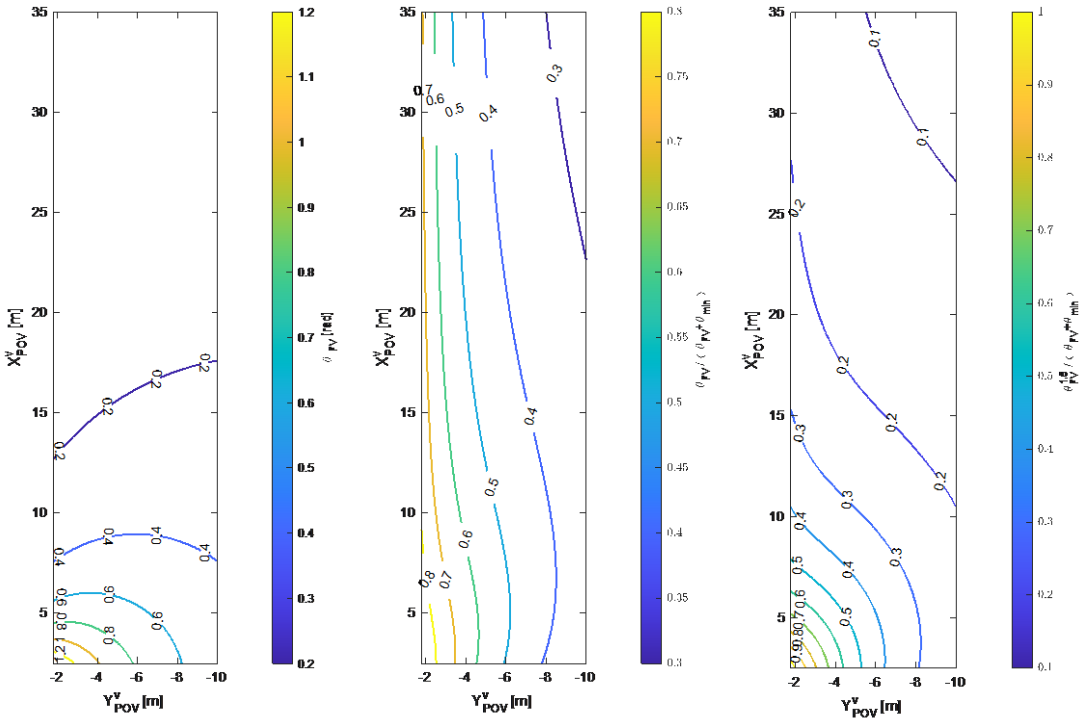

(a) *(b)* *(c)*

Figure 20 Angles

Figure 20 (a) and (b) are showing the magnitude of θ_{FV} and proportion of θ_{FV} with different (artificially "simulated") POV positions (relative to the ego vehicle). The x and y axes represent the distance between the POV's centre of gravity and the middle of the EGO vehicle's front bumper in longitudinal and lateral direction respectively, i.e., the origin is the middle point of EGO vehicle's front bumper. The magnitude of θ_{FV} increases as the longitudinal range between POV and EGO vehicle decreases, and the proportion of θ_{FV} increases as the lateral range between POV and EGO vehicle decreases. A combination factor of these two items, calculated using the following equation, can represent how critical the situation is depending on the POV position.

$$F = \frac{{\theta_{FV}}^{k_1}}{\theta_{FV} + \theta_{min}} \tag{20}$$

where k_1 is a free model parameter and an example of the combination factor with $k_1 = 1.5$ is visualized in Figure 20 (c). The combination factor F can not be used directly as a perceptual input because it is a measurement solely depending on the position of the

POV while ignoring the effect of speed. Taking the derivative of F into consideration, the perceptual input was calculated as:

$$P(t) = \ k_2 \cdot F + k_3 \cdot \dot{F} = k_2 \cdot \frac{{\theta_{FV}}^{k_1}}{\theta_{FV} + \theta_{min}} + k_3 \cdot \left(\frac{\dot{\theta_{FV}}^{k_1}}{\theta_{FV} + \theta_{min}} \right) \tag{21}$$

Hence in Model 3, $p(t)$ can be expressed as:

$$p(t) = \begin{cases} k_2 \cdot \frac{{\theta_{FV}}^{k_1}}{\theta_{FV} + \theta_{min}} + k_3 \cdot \left(\frac{\dot{\theta_{FV}}^{k_1}}{\theta_{FV} + \theta_{min}} \right), & \text{before POV} - \text{in} - \text{lane} \\ \frac{\dot{\theta}_{FV}}{\theta_{FV}}, & \text{after POV} - \text{in} - \text{lane} \end{cases} \tag{22}$$

2.3.4 Kalman Filter for predicting derivatives

The value of derivatives, including $\dot{\theta}_{FV}$ in Model 1, $\dot{d}_{y,pov2lane}$ in Model 2 and $\dot{F}$ in Model 3, were calculated using Kalman filters, because the results of differentiating θ_{FV}, $d_{y,pov2lane}$ and F can be quite noisy. Kalman filters can estimate the state of a process given noisy observations. The states variables are x and $\dot{x}$, where x represents θ_{FV}, $d_{y,pov2lane}$ or F in Model 1, 2 or 3 respectively and $\dot{x}$ represents the derivative of x, i.e. $\dot{\theta}_{FV}$, $\dot{d}_{y,pov2lane}$ or $\dot{F}$. The process model can be expressed as:

$$\begin{bmatrix} x_{n+1} \\ \dot{x}_{n+1} \end{bmatrix} = \begin{bmatrix} 1 & \Delta T \\ 0 & 1 \end{bmatrix} \times \begin{bmatrix} x_n \\ \dot{x}_n \end{bmatrix} + \omega(n) \tag{23}$$

where n is the time step and the $\omega(n)$ represents the state error, which is zero mean gaussian noise. The measurement model can be expressed as:

$$x_{n,measure} = [1 \ \ 0] \times \begin{bmatrix} x_n \\ \dot{x}_n \end{bmatrix} + v(n) \tag{24}$$

where $x_{n,measure}$ is the noise observation of x_n, i.e. measurement value of θ_{FV}, $d_{y,pov2lane}$ and F from ESmini, and $v(n)$ represents the measurement error, which is also zero mean gaussian noise. The covariance matrix of states error, denoted as Q, was set to:

$$Q = \begin{bmatrix} 0 & 0 \\ 0 & 0.1 \end{bmatrix} \tag{25}$$

The covariance matrix of measurement error was denoted as R. Because there was only one measurement variable in each filter, R is a single value rather than a matrix. The R values for filters with different measurements are shown in Table 2.

Table 2 R values

Measurement	R
θ_{FV}	0.25
$d_{y,pov2lane}$	0.25
F	0.5

Figure 21 depicts one example of each filter. The measurement values are shown in left plots, and the derivatives from the Kalman filter and differentiating are shown in right plots. As can be seen, there are some overshoots in the Kalman filter output, which possibly could be improved (partially removed) by applying a median filter before the Kalman filter.

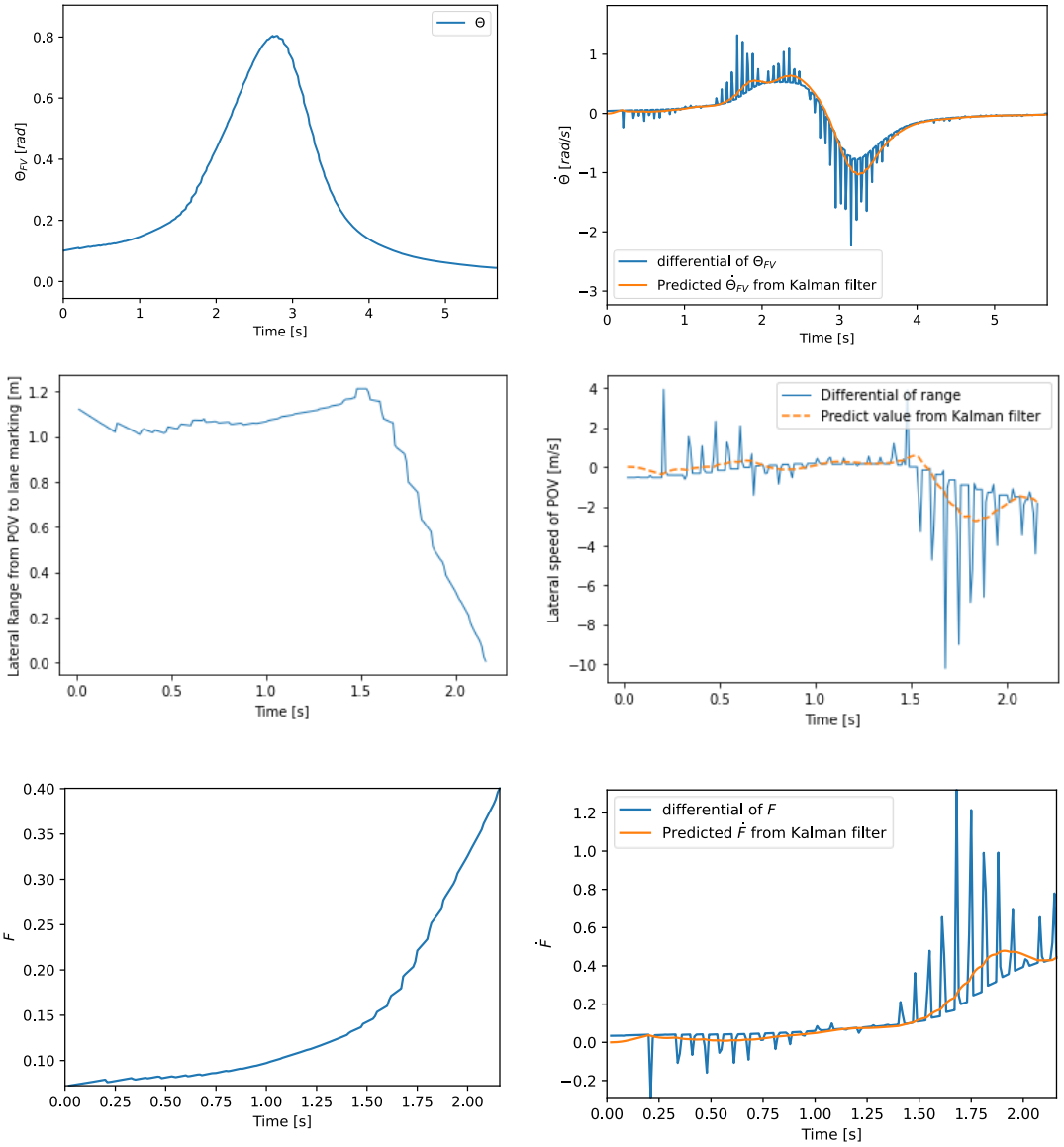

Figure 21 Kalman filter

2.4 Parameters Optimization

There is multiple optimization method that can be used to optimize parameters in models. PSO algorithm optimization technique, developed by Eberhart and Kennedy was introduced 1995 based on behaviour of animal group (Almeida & Leite, 2019). In this thesis, Particle Swarm Optimization, or PSO, was chosen as it also was used in Svärd et al. (2020) and have previously been shown to provide relatively good parameter fitting with relatively few simulations.

PSO will run the simulation multiple times and each time with different values for the parameters to be fitted. This will lead to several different result and different responses from the driver (model). This is done iteratively until the driver model have a response as similar as possible to the real human driver, as captured by the data the model is fitted to. There is one problem with this kind of training. Because of the complexity of the driver model, large variety and number of free parameters that need to be optimized (in our model), the training requires a lot of computing time and computer power. Because this thesis was limited in time and computer resources, finding new solutions was necessary to reduce training time. One quick solution was to decrease number of training iterations, but this can lead to bad result due to lack of training. To avoid this problem and maximize the available time, three solutions were tested and are present below:

- Define proper boundaries (as narrow as possible, but not too narrow)
- Fix the values for some parameters, based on previous work or a pre-simulation
- Python multi-core processing (as we used Python)

Defining the "correct" range of boundaries will decrease the search area, which will decrease the time to find the optimal value. This can be done in a couple of different ways; one is to calculate the feasible and not feasible area. Second is to know the search area from the beginning and define boundaries manually. In the end, the boundaries was chosen from Svärd et al. (2020). Putting fixed values from some parameters will decrease the computing time as fewer parameters needs to be fitted, and it will allow for increasing the resolution and range on the other parameters, increasing the chances to find optimal values for other important parameters. The last solution is to use multi-core processing. We used Python as the simulation framework and consequently we tried Python multiprocessing. This enables the training to be divided into smaller sub-tasks, which will enhance the computing time greatly. The selected events were divided into two separate datasets, see Figure 22. One was used for training and other for test. The training set contains 70% of the events while test only 30% of the events.

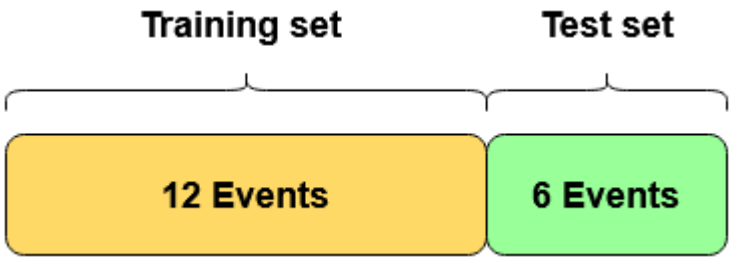

Figure 22 Dataset for training and test

2.4.1 Cost function

The cost function introduced in Svärd et al. (2020) requires repeated simulations to generate the distribution of t_B and j_B. A fairly large number of particles and iterations are necessary due to high complexity of the model. Hence, a large amount of repeating simulations for calculating cost will lead to an extremely high computing time. In order to save computing time, the optimization in this thesis was divided into three steps. In step 1 and 2, PSO was performed without noise, i.e., $\sigma = 0$, using Least Mean Square (LMS) method to produce a rough optimized parameter set. One is for minimizing the

LMS error of t_B, while the other one is for minimizing the LMS error of j_B. Finally, the parameters were restricted to a very narrow boundary around the optimised result from first two steps and then PSO was carried out with noise using maximum likelihood estimation. The original plan was to fix some parameters before training with noise. Due to limited time (due to late identification of the error/offset in the annotated data), it was not possible to do that. Instead of reducing the complexity of the model, we perform PSO with narrow boundaries. Because the boundaries are narrower, a smaller particle size and fewer iterations are required, resulting in a substantial reduction in computing time, but where the true value may lay outside the range. The cost function calculations for each step are described in detail in the following part of this section.

2.4.1.1 Acceleration fitting

The reference value $t_{B,i,ref}$ and $j_{B,i,ref}$ were obtained from the estimate from the model fitting to the SHRP2 near-crash data. An approach and MATLAB code of fitting the acceleration into a piecewise linear function was introduced in Bärgman (2019). The piecewise linear function contains 3 segments. The acceleration is kept constant at beginning, and then drops linearly from time t_B with jerk j_B to a final level of deceleration. The starting and end point of data for fitting is crucial. The model fitting was performed two times to get the value of t_B and j_B. In the first-time model fitting, as shown in Figure 23(a), acceleration data from the start of event until the maximum deceleration were chosen to ignore the effect of acceleration starting to increase again. Figure 23 (b) shows the second model fitting. The start point was adjusted to 1.5 s before the t_B, resulted from the first model fitting, to find the time when driver start to decelerate sharply.

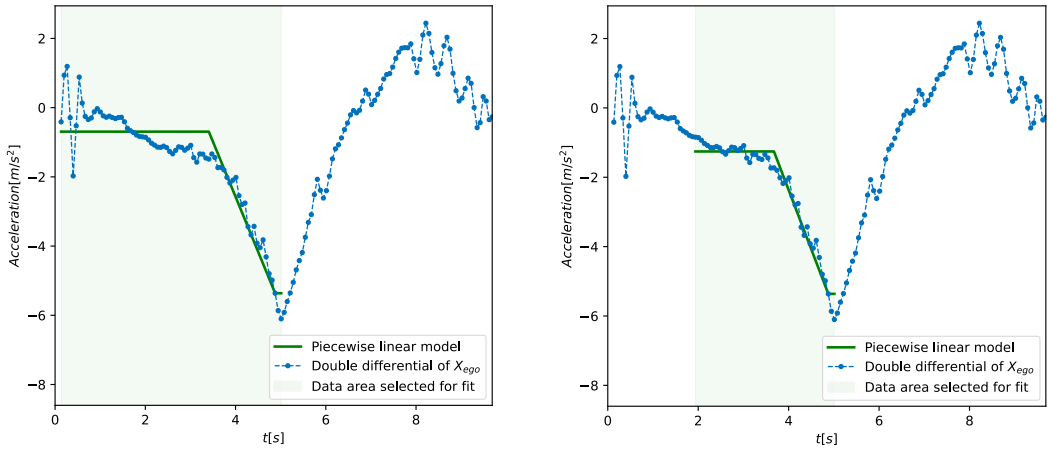

(a)1st fitting *(b)2nd fitting*

Figure 23 Acceleration fitting

2.4.1.2 Training without noise

Instead of piecewise linear fitting, the driver model output t_B was set to the time of first intervention from the driver model. The acceleration reached the final level at t_E, as shown in Figure 24. The jerk j_B was calculated as:

$$j_B = \frac{a_0 - a_1}{t_E - t_B} \tag{26}$$

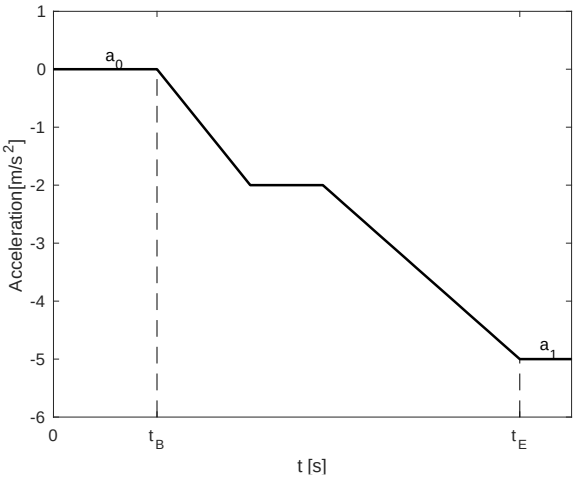

Figure 24 Acceleration output from driver model

The time of first intervention only depends on parameter K, M, C for model 1, or K, M, C, k_{pre}, k_{dx} for model 2, or K, M, C, k_1, k_2, k_3 for model 3, which were the free model parameter on optimization step 1. Repeating simulations are not required because σ was 0 and the result would be same for same event with same parameter set. The cost function was the average mean normalised square error of brake onset timing.

$$cost = \frac{1}{N}\sum_{i=1}^{N}\left(\frac{t_{B,i} - t_{B,i,ref}}{\max t_{B,ref} - \min t_{B,ref}}\right)^2 \tag{27}$$

All the optimised parameter from step 1 were fixed, then k and A_r were the free model parameters on step2, and the cost function was the average mean normalised square error of jerk.

$$cost = \frac{1}{N}\sum_{i=1}^{N}\left(\frac{j_{B,i} - j_{B,i,ref}}{\max j_{B,ref} - \min j_{B,ref}}\right)^2 \tag{28}$$

When the driver model did not respond or a collision was not avoided, the cost was set to a large value (100). Because the driver model will be used in Monte Carlo simulations with zero-mean gaussian white noise, the values of t_B and j_B are likely to centre around the value when the noise is zero. As a result, if there was no response from the driver model or the collision was not avoided when noise is zero, it is highly likely that similar results would be obtained from noise simulations. The parameters from PSO training with LMS cost function were used to generate the boundaries for final PSO training with maximum likelihood cost function.

2.4.1.3 Training with noise

The cost function in Svärd et al. (2017) was adopted for training with noise, which is the total log likelihood of the parameter set $\mathbb{P}_{j.k}$, with compensation of potential outlier, which is shown in Equation 5:

For each event, with each parameter set, the simulation was repeated 200 times with noise to get the driver model response output. The values of brake onset timing and jerk

from driver model were used to generate a 2D probability distribution using gaussian Kernel Density Estimation. The kernel size was chosen with Scott's method initially as Equation 29.

$$BW = \sigma \cdot n^{-\frac{1}{d+4}} \tag{29}$$

where d is the number of dimension and n is number of samples ($d = 2, n = 200$). In Svärd et al. (2017), the kernel size of t_B and j_B were chosen to prioritize a good fit of t_B, since t_B is less dependent on vehicle dynamics. In this thesis, the kernel size was changed to make the ratio of the variance of generated distribution was that the twice of the ratio of the variance of driver model's output values, to generate a skewed distribution.

$$\frac{\sigma_{j_{B,kde}}^2}{\sigma_{t_{B,kde}}^2} = 2 \times \frac{\sigma_{j_B}^2}{\sigma_{t_B}^2} \tag{30}$$

The final kernel sizes of t_B and j_B were:

$$BW_{t_B} = \sigma_{t_B} n^{-\frac{1}{d+4}} \tag{31}$$

$$BW_{j_B} = \sqrt{2} \times \sigma_{j_B} n^{-\frac{1}{d+4}} \tag{32}$$

3 Result

Each model's parameter set was optimized using the same training set. Steps 1 and 2 of optimization, i.e., training without the noise item, were repeated three times for each model to check if the PSO algorithm produced was a local minimum. Step 1 was performed with 20 particles and 50 iterations, while Step 2 was performed with 20 particles and 30 iterations, due to fewer parameters in the model. Because the LMS errors do not completely represent model fitness, the optimal parameters were used to run Monte Carlo simulations to compute the total likelihood and AIC of optimal parameters from each model. The total log likelihood and AIC were used to compare performance of the different models. The model with highest total log likelihood and lowest AIC was chosen and tested on the test set and it was used to perform PSO training with noise.

3.1 Training without noise

3.1.1 Model 1 - without noise

Table 3 shows the optimal parameters of Model 1 from training without noise. In all three repeated PSOs, the value of gain K got saturated to the maximum of the chosen range, and the value of sum of non-looming evidence for or against braking M got saturated to the minimum of the chosen range.

Table 3 Optimal parameters of Model 1 from PSO without noise

PSO Run	No. of events in training set	K	M	C	k	A_r
1	12	40.000	0.000	0.549	4.165	1.000
2	12	40.000	0.000	0.000	4.138	0.960
3	12	40.000	0.000	0.295	4.274	1.000

Figure 25 shows an example event using Model 1. As can be seen, $P(t)$ and activity remains zero before target-in-line, whereas after POV-in-lane, $P(t)$ begins to rise, the activity quickly reaches the threshold 1 and the driver model applied harsh braking.

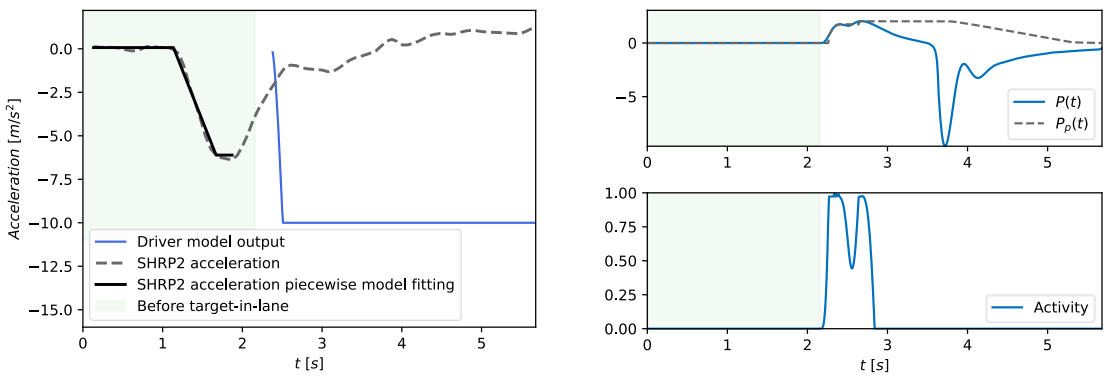

(a) *(b)*

Figure 25 Model 1 response

3.1.2 Model 2 - without noise

Table 4 shows the optimal parameters of Model 2 from training without noise. In all three repeated PSO, the value of gain K got saturated to the maximum of the chosen range, and the value of sum of non-looming evidence for or against braking M got saturated to the minimum of the chosen range.

Table 4 Optimal parameters of Model 2 from PSO without noise

Run	No. of events in training set	K	M	C	k_{pre}	k_{dx}	k	A_r
1	12	40.000	0.000	0.977	5.000	2.296	3.217	0.911
2	12	40.000	0.000	0.200	5.000	3.084	4.184	0.910
3	12	40.000	0.000	0.086	6.151	4.015	4.420	0.924

Figure 26 shows the same example event using Model 2. As can be seen, the driver model began to respond before POV-in-lane. $P(t)$ fell to zero at POV-in-lane timing, and a negative $\mathcal{E}(t)$ value ($P(t) < P_p(t)$) was accumulated, resulting in a substantial drop-in activity.

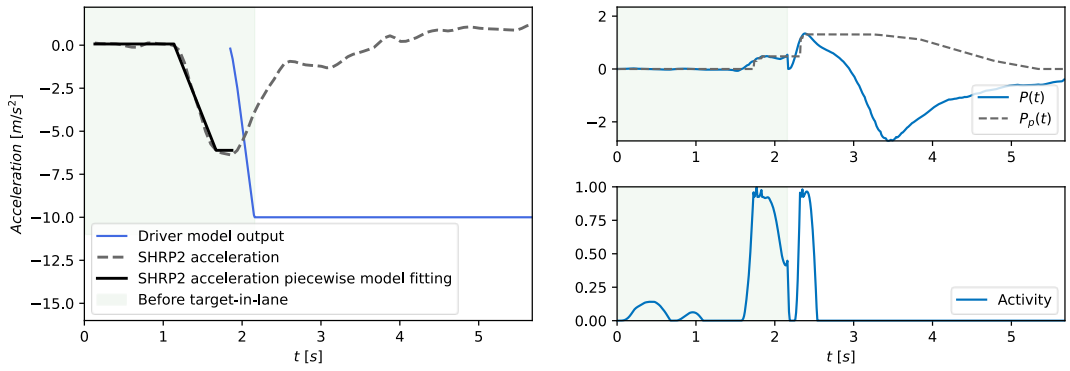

(a) *(b)*

Figure 26 Model 2 response

$P(t)$ was calculated as $\frac{\dot{\theta}_{FV}}{\theta_{FV}}$ after POV-in-lane, the full vehicle angle θ_{FV} was only monitored after POV-in-lane. The Kalman filter, used to calculate $\dot{\theta}_{FV}$, requires time to converge to the real predicted value and initial guess value was set to zero (as shown in Figure 27). Hence $P(t)$ dropped to zero at POV-in-lane timing.

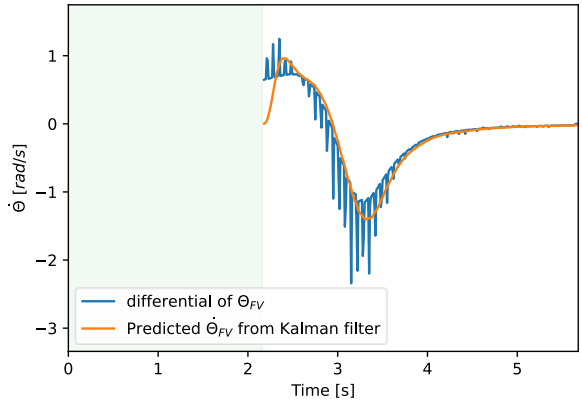

Figure 27 Kalman filter

3.1.3 Model 3 - without noise

The optimal parameters of Model 3 are shown in
Table 5. The optimal values of k_2 were zero in all three PSO runs. And k_2 , the scaling factor of magnitude of F, was then removed from Model 3. $P(t)$ can be computed as the linear scaling of $\dot{F}$.

$$P(t) = k_3 \cdot \dot{F} = k_3 \cdot \left(\frac{\dot{\theta_{FV}}^{k_1}}{\theta_{FV} + \theta_{min}} \right) \quad (33)$$

Table 5 Optimal parameters of Model 3 from PSO without noise

Run	No. of events in training set	K	M	C	k_1	k_2	k_3	k	A_r
1	12	12.000	2.225	0.000	1.804	0.000	4.265	1.046	0.954
2	12	22.954	6.847	0.076	2.000	0.000	5.839	0.860	0.902
3	12	29.878	8.000	0.002	1.995	0.000	5.065	1.081	0.931

Figure 28 depicts the same example event using Model 3. The driver model began to respond before POV-in-lane. There was also a decrease in $P(t)$ at POV-in-lane timing because the calculation of $P(t)$ changed from F to full vehicle angle looming. The decrease in $P(t)$ was not caused by a sudden change in situation, but rather by a change in calculation approach. In the event shown in Figure 28 there was substantial difference between the $P(t)$ value calculated with different approach at POV-in-lane timing. After POV-in-lane, the value of $P(t)$ decreased below the predicted value $P_p(t)$ and perceptual error became negative resulting in decreasing in activity. Figure 29 shows an example event in which the value of $P(t)$ did not change much after POV-in-lane, and activity continued to rise because $P(t)$ remained above the predicted value $P_p(t)$.

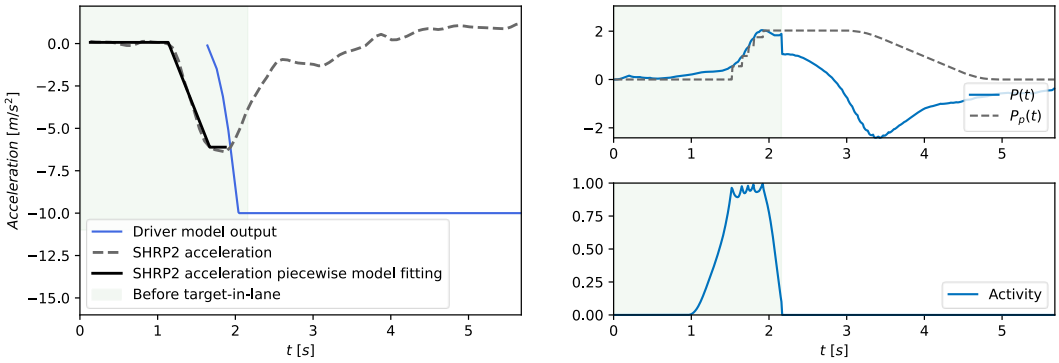

(a) *(b)*

Figure 28 Model 3 response-example 1

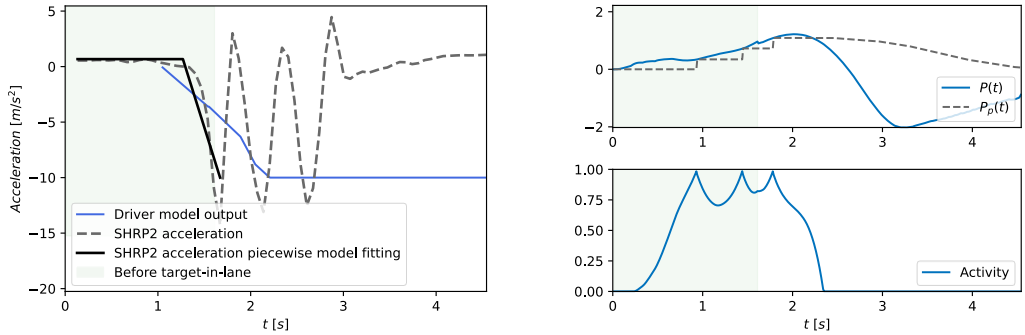

(a) *(b)*

Figure 29 Model 3 response - example 2

3.1.4 Model comparison

All the 12 events were simulated without noise using the optimal parameters from each model. The errors of t_B and j_B were calculated as the discrepancy between the driver model output and the reference value from SHRP2. Figure 30 and Figure 31 are showing the t_B and j_B errors of different models. Every box contains the errors from all the 12 training events. The positive value of t_B error represents the driver model responding later than human driver, and the positive value of j_B error represents the driver model braking more gently than the human driver.

As can be seen, the performance of each model was relatively unchanged. Model 1 produced the most imprecise results, and it started to brake much later and more harshly than the human drivers. The performance of Model 2 was better than Model 1. The t_B error of Model 2 error was almost evenly distributed on both the positive and negative sides but with a large error, i.e., it started braking later than human drivers in some events and earlier in others. In Model 3, t_B errors were centred around zero and had substantially more narrow spread comparing to Model 1 and 2. For the jerk, the errors were centred around zero but with a relatively large spread (±20 m/s^3).

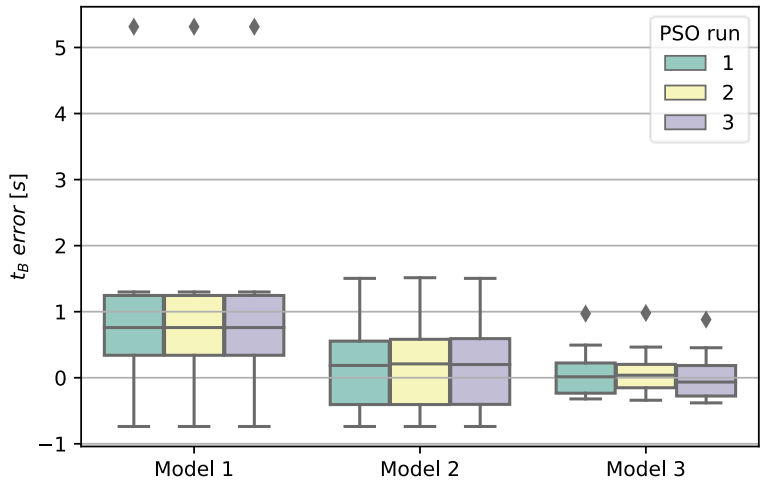

Figure 30 Break onset timing error

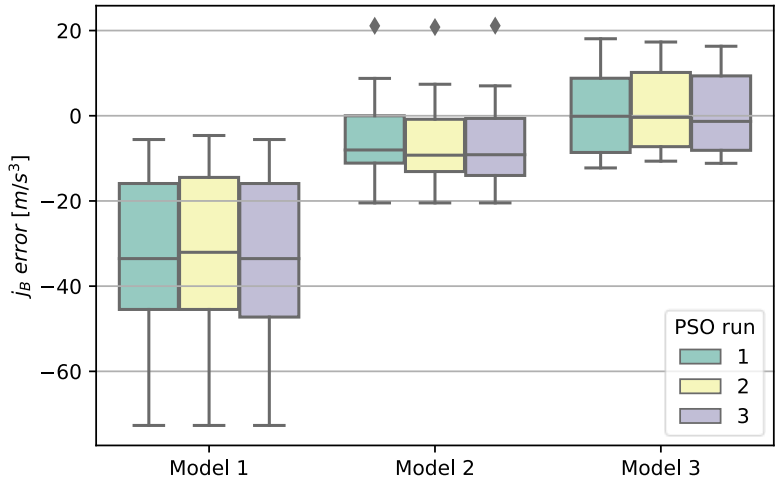

Figure 31 Jerk error

To compare the models' performance with noise, the optimal parameters from PSO training without noise were used to calculate the total log likelihood. the noise standard deviation (σ) was set to 0.97 (from optimal value of base model in Svärd et al. (2020)). The Akaike information criterion (AIC) of the different models was calculated to estimate the quality of each model, relative to each other. AIC rewards goodness of fit and penalize high model complexity. In this thesis, the AIC was calculated as:

$$AIC = 2 \cdot k_p - \sum log(\mathcal{L}) \tag{34}$$

where k_p is the number of parameters. Even if σ was fixed to 0.97, it was also included in the free model parameters. Because σ will eventually be optimized in training with noise. The purpose was to compare the performance of each model under the assumption that the optimal value of σ was 0.97 to select the best model for training with noise.

Table 6 Model compare

Model	No. of training set	No. of Parameters	Run	$\sum log(\mathcal{L})$	AIC
Model 1	12	6	1	-82.868	94.868
			2	-82.675	94.675
			3	-82.899	94.899
Model 2	12	8	1	-57.415	73.415
			2	-56.445	72.445
			3	-57.065	73.065
Model 3	12	8	1	**-56.037**	**72.037**
			2	-56.534	72.534
			3	-62.342	78.342

As shown in Table 6, despite having the smallest parameter set size, Model 1 had the highest AIC due to the low total log likelihood (as expected as Model 1 really was not a proper cut-in model, as it did not consider driver activation before the POV entered the EGO vehicle lane). Models 2 and 3 had comparable total log likelihood and AIC values. However, when it came to driver model response of each event, the performance of Model 3 was better than Model 2. Because the $t_{B,max}$ and $j_{B,max}$ in Model 2 were small in some events, resulting in a high value in compensation part of the log likelihood according to Equation 5. The parameters from Model 3's first PSO run provided the best model performance, with the highest total log likelihood and lowest AIC, making it the best model.

3.1.5 Results from the best model – Model 3

Figure 32 shows some good model response events from the training set, using parameters from Model 3's first PSO run. The acceleration from SHRP2, the piece-wise linear fitting of SHRP 2 acceleration and the driver model response from 200 Monte Carlo simulations are plotted in the upper plot of each sub-figure. The lower plot is corresponding 2D probability density of t_B and j_B. The black dot markers represent the scatter of t_B and j_B of driver model output from 200 Monte Carlo simulations used to generate the 2D probability density distribution. The red cross marker is $t_{B,ref}$ and $j_{B,ref}$ from piecewise linear model fitting of SHRP2 acceleration. The driver model response for all the events in training set are shown in Appendix.

Figure 33 shows an event with low log likelihood. As can be seen, the driver responded later than a human driver. A collision had been avoided by driver model, but the longitudinal range between POV and EGO vehicle was smaller than real-world situation from SHRP2, as shown in Figure 34.

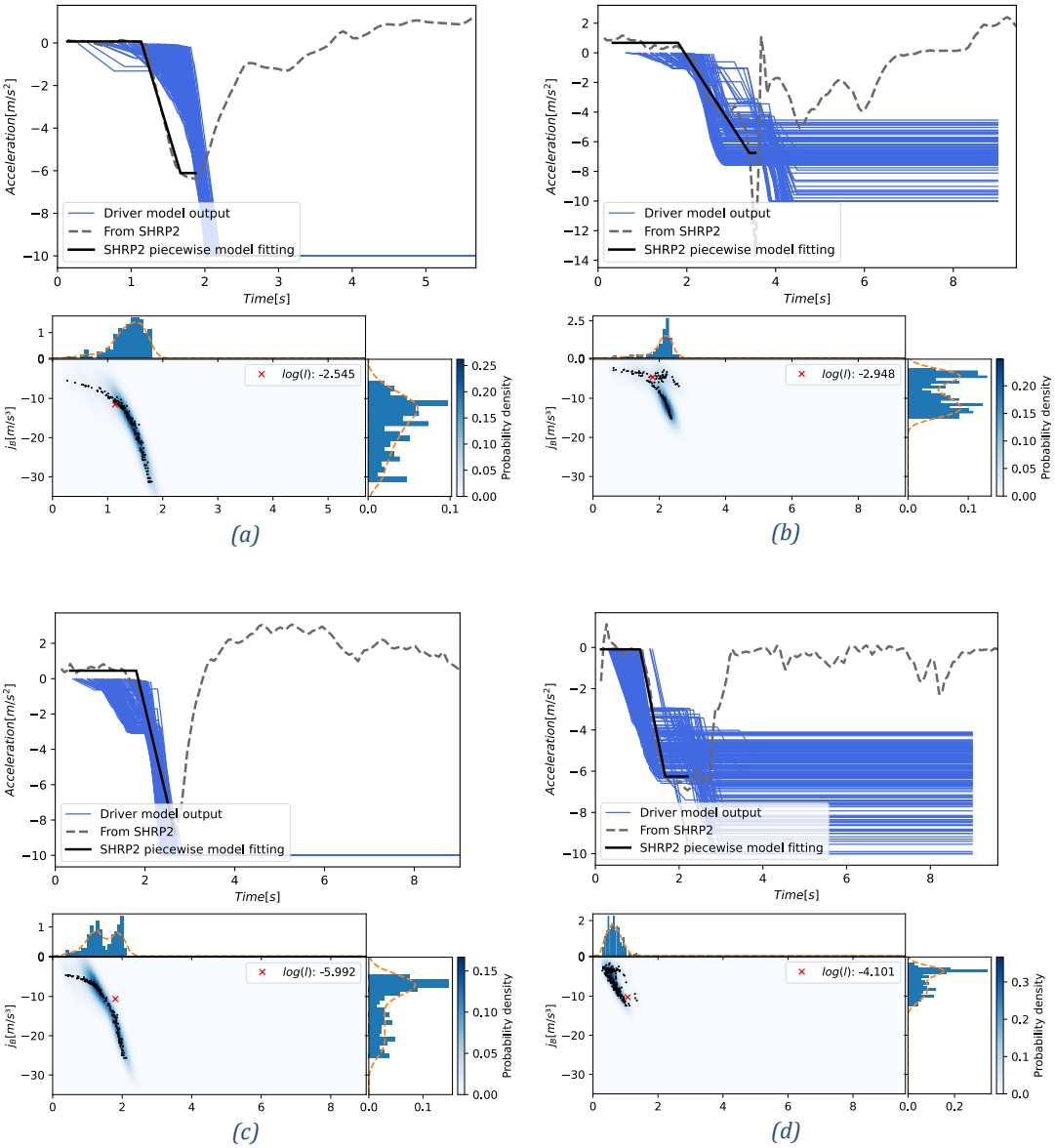

Figure 32 Good training result with model 3

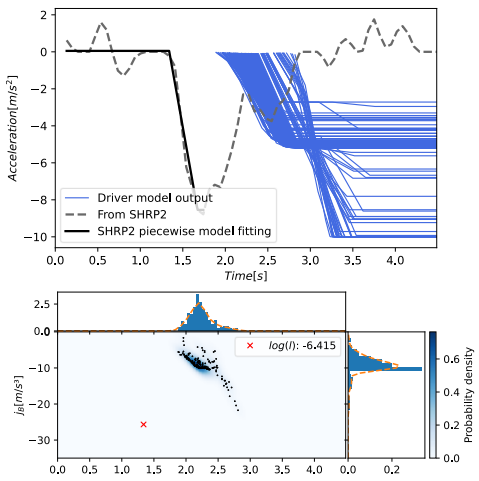

Figure 33 Event with low log likelihood

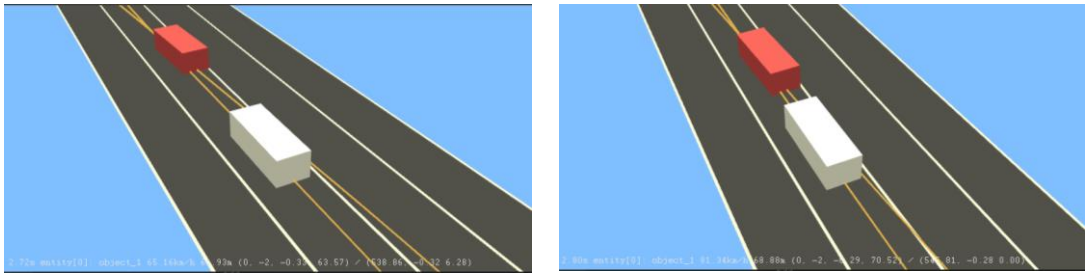

(a) Human driver response *(b) Driver model response*

Figure 34 Compare driver model with human driver in event with low log likelihood

We tested the Model 3 performance by running 200 Monte Carlo simulations using the test set with $\sigma = 0.97$ (from Svärd et al., 2021). The total log likelihood was -20.469. There are six events in test set. The average log likelihood of test set was -3.412, while the average log likelihood of training set was -4.670. The results of test set are shown in Appendix.

3.2 Training with noise – Model 3

Model 3 was used to perform PSO training with noise, and the boundaries of parameter were set around optimal parameter result from 1st run. Some main parameters were limited to a narrow boundary (as shown in Table 7), while other parameters were fixed to the optimal result from training without noise. The same 12 events were used as training set with 10 particles and 25 iterations. The driver model response for each event from training/test sets are shown in Appendix.

Table 7 Parameter boundaries for training with noise

Parameter	K	σ	k	k_1	k_3
Boundary	11.5 – 12.5	0.9 – 1.0	0.94 – 1.14	1.70 – 1.90	4.06 -4.46

The optimal parameters are shown in Table 8. The optimal parameters for training with noise were slightly different from those for training without noise, resulting an increase in the total log likelihood from -56.037 to -49.114 (as shown in Table 9). The total loglikelihood of the test set increased from -20.469 to -19.787.

Table 8 Optimal parameter of Model 3 from training with/without noise

Training	K	M	C	k_1	k_3	k	A_r	σ
Without noise	12.000	2.225	0.000	1.804	4.265	1.046	0.954	0.970
With noise	12.002	2.225	0.000	1.867	4.134	0.981	0.954	0.946

Table 9 Performance of Model 3 after training with/without noise

	Events	$\sum log(\mathcal{L})$	$ave\left(\sum log(\mathcal{L})\right)$	AIC
Without noise	Training set	-56.037	-4.670	72.037
	Test set	-20.469	-3.412	-
With noise	Training set	-49.114	-4.093	65.114
	Test set	-19.787	-3.29	-

In Svärd et al. (2020), 56% of events with good overall model fit can be validated through using log-likelihoods, brake onset timing errors and jerk errors. The events were "considered" good if the models fulfilled two conditions:

- Individual log likelihood > -4.5
- 50% of the simulations had brake onset timing error within ± 0.6s and jerk error within ± 4.6m/s^3

The dataset is relatively small in comparison to previous work where only 18 events was used for the study in this thesis. Model 3 performance had 66.7% events (12/18) with loglikelihood > -4.5 and 50% (100/200) simulations (with lower brake onset timing).

Figure 35 shows the results of Model 3. The blue line (with histogram) is the KDE of results from 100 simulations of all the good fit events. The rests of the lines are the KDE of results from 100 simulations of each good fit events. Model 3 showed promising result on the brake onset timing part where the model performed within ± 0.6s, see Figure 35 (a). But the brake jerk showed opposite result where the model performed outside the range of ± 4.6m/s^3, see Figure 35 (b).

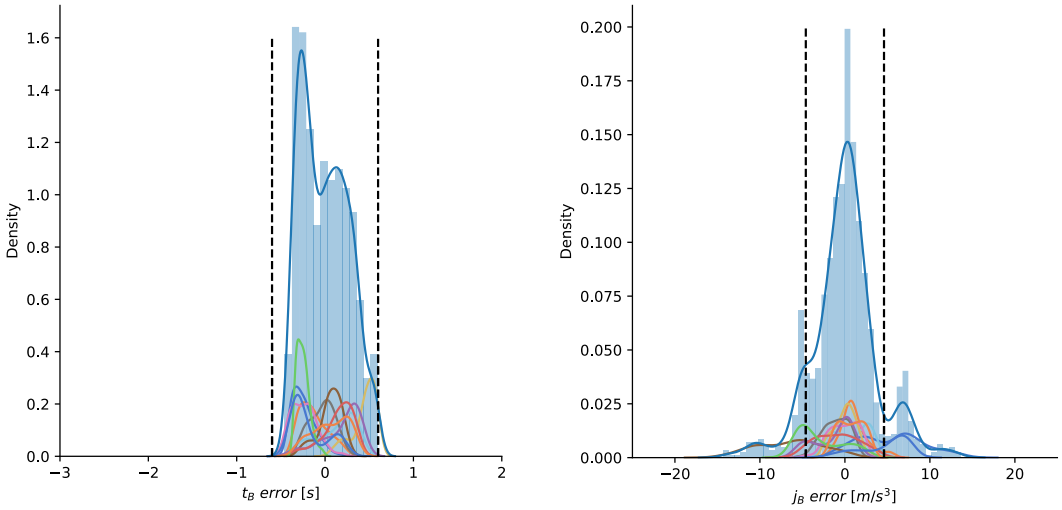

(a) *(b)*

Figure 35 Events with good fitness

4 Discussions

This research aims to develop a driver model of driver brake responses in cut-in scenario and to fit parameters to and compare the driver model response in computer simulations with the human driver response from the original cut-in events, reconstructed from videos of near-crashes in the SHRP2 naturalistic driving study. Four different computational models were developed, based on an existing rear-end accumulation driver model in Svärd et al. (2017, 2020). The differences between those models and the original rear-end model was the calculation of the perceptual input $P(t)$. Models 1, 2 and 3 were implemented in the virtual simulation framework used (which use the tool esmini and Python). The model parameters were optimized using Particle Swarm Optimization (PSO) to fit the model to the driver break onset timing and break jerk in a set of near-crashes extracted from the SHRP2 naturalistic driving study (Virginia Tech Transportation Institute, 2020). Model 4 was proposed but never tested, due to limited project time (therefore it was left for future investigation).

Models 1, 2 and 3 were using different perceptual input based on if the vehicle to cut in had entered the ego vehicle lane or not (before/after POV-in-lane). *Before POV-in-lane* denotes that the POV is completely outside the EGO vehicle's lane, whereas *after POV-in-lane* denotes that the POV has reached the lane marking or is in the same lane as the EGO vehicle, see Figure 13. In Model 1, $P(t)$ was set to zero before POV-in-lane. It thus only started to accumulate looming error after POV-in-lane, and $P(t)$ after POV-in-lane was calculated with looming using full vehicle angle. Model 2 and 3 used the same $P(t)$ calculation as Model 1 for the after POV-in-lane condition, with additional $P(t)$ calculations performed before POV-in-lane. Before POV-in-lane, $P(t)$ in Model 2 was calculated using inverse time to lane crossing (TLC) while also taking longitudinal range into account. In Model 3, two angles were investigated, the full vehicle angle and the angle between the POV's corner and the longitudinal direction. According to the patterns of those two angles in the cut-in scenario, a mathematical equation was created to calculate $P(t)$. The optimization process was divided into training, one training with noise and one training without noise. Models with the best performance were proceeded training with noise and Model 3 was selected for this part. The training with noise was performed with $\sigma = 0$ to minimize the least mean square error of break onset timing and jerk.

4.1 Interpretation of results

Given the method described above, we interpret the results as follows. In section 4.1.1, the results of different models are interpreted and compared. Section 4.1.2 discuss possible reasons why the driver model does not fully capture the driver's response behaviour.

4.1.1 Compare the models

From the training without noise result, the values of accumulation gain K were very high (got saturated to the maximum of the chosen range) due to P(t) being set to zero before POV-in-lane and consequently causing very high activity level when the POV enters the EGO lane at the last moment (when looming already is very high), resulting in the driver having to brake harshly to avoid collision. The driver model brake response was delayed 1-1.5 second compared to the real driver brake responses. Model 1 consequently performance quite poorly, with the responses all

being very large. This was expected because in a real-case scenario, the driver will typically (if he/she is attentive) already act before the POV enters the lane, depending on the situation.

Model 2 had better performance compared to model 1. Adding the additional predictor of inverse of time to lane crossing, the driver did have a better braking response and more "smooth" braking. Model 2 accumulate the perceptual input related to the lateral and longitudinal distance of the POV and EGO, which is a component that we considered having potential to mimic driver's judgement about if the situation is critical or not. This additional predictor did improve Model 2 overall performance, compared to Model 1, because the driver Model 2 can act before POV-in-lane, which resembles a real driver response, which Model 1 did not. However, the results were still substantially different from that of the original events (the real driver braking response), with a 0.8-0.9 second delay. Due to the Kalman filter being initiated after POV-in-lane, the value of $P(t)$ dropped to zero at POV-in-lane timing, which resulted in a discontinuity in activity. The solution could be starting the Kalman filter earlier to provide enough time for the filter to converge. Another reason for the poor model performance could be that directly adding a linear scaling of longitudinal range on the denominator with inverse time to lane crossing does not adequately capture how a human driver response.

The performance of Model 3 was slightly better than Model 2 with only an average of 0.5 second delay in braking response, compared to the real drivers. The brake jerk error between the driver model output and human driver response was large. In Model 3, the value of $P(t)$ was not 'smooth' at POV-in-lane timing because the calculation equations were different before and after the POV-in-lane, and it might result in a large change in activity level. The sudden change in activity at POV-in-lane timing was caused by using different calculation equations before and after POV-in-lane, rather than a sudden change in situation (e.g., urgent braking/accelerating of POV). It is difficult to smooth it by scaling the first part to fit the magnitude of the second part. Assigning a scaling factor to each time step is difficult because it is impossible to predict when the POV will reach the lane mark. One possible solution that could help in this situation is to shift the $P_p(t)$ by the same amount as the change in $P(t)$, to ensure that $\varepsilon(t)$ does not change when changing equations. $\varepsilon(t)$ is the error between $P_p(t)$ and $P(t)$, which was accumulated in each timestep. As a result, there will still be a discontinuity in $P(t)$, but it will have little effect on the activity.

To estimate the model's performance with noise, the three models (with optimal parameters from training without noise) were tested with noise $\sigma = 0.97$ (from optimal value of base model in Svärd et al. (2020)). For each model, Monte Carlo simulations were performed, and the total loglikelihood and AIC of each model were calculated to assess the model performance with noise. Model 3 provided the highest total log likelihood and lowest AIC. Hence Model 3 had the best performance after training without noise and we chose to run optimization with noise for this model.

After training Model 3 with noise, the total log likelihood for both the training and the test sets were slightly better than training without noise. The final average log likelihood of the training set was -4.093 and the final average log likelihood of the test set was -3.29. The brake onset timing from 200 Monte Carlo simulations were approximately within ±1 second from human driver for 8/12 events in training set and 4/6 events in test set. All events in training set had brake onset timing errors within ±2

seconds and all events in test set had brake onset timing errors ± 1.5 seconds. The model performance on jerk was even poorer. The jerk errors were within ± 20 m/s^3 for 10/12 events in training set. The jerk errors of some Monte Carlo simulations from the remaining two events in training set were slightly above 20 m/s^3. The jerk errors of 5/6 events in test set were within ± 15 m/s^3, and the jerk errors were slightly above 15 m/s^3 for the remaining event in test set. In summary, even if Model 3 was the best model, the overall performance of Model 3 was simply not good enough for its intended use. Compared to the reduced-complexity rear-end model in Svärd et al. (2020), Model 3 had the similar performance on break onset timing, while the jerk errors in Model 3 were larger than the rear-end model in Svärd et al. (2020). As mentioned in result section, we compare the model performance with Svärd et al. (2020) in terms of log likelihood. However, it is really hard to tell if the model is good comparing to rear end model in Svärd et al. (2020) , because it is not obvious which method should be used to compare models.

4.1.2 Likely reasons to why the driver model does not fully capture the driver's behaviour

There are many possible reasons why the driver models did not capture the behaviours of the real-world (original event) drivers. Data quality, the parameter fitting, and/or the predictors and components of the driver model are the most likely suspects. In the following we discuss these potential issues in turn.

Data quality

There were events with low video resolution and annotators have to sometime assume the POV current position, which can lead to an "incorrect" trajectory. When the longitudinal range is large, the uncertainty of the lateral range result from the annotation tool is high, resulting in poor data quality. Even if the data was manually modified, good data quality cannot be guaranteed because the modified ranges were measured from the front view video with eyes-only-based adjustments.

Parameter fitting (the optimization process)

In Model 1 and 2, the value of accumulation gain K was saturated to the maximum of the selected range, while the value of the sum of non-looming evidence for or against braking M was saturated to the minimum of the selected range. To reach the threshold faster, both Model 1 and Model 2 tended to have a higher change rate of activity. Because the driver model in Model 1 does not react before POV-in-lane, and activity in Model 2 drops to zero at POV-in-lane timing, the break onset timing errors may become smaller as the change rate of activity increases. If the boundaries were wider, the value of K would increase and the value of M will decrease, resulting in a quicker change in activity (as Equation (1)). However, it will not substantially improve model performance. Regardless of how quickly activity changes, Model 1 will not react earlier than POV-in-lane timing. To achieve a better and more 'stable' performance in Model 2, it is preferable to fix the discontinuity problem in $P(t)$ rather than having a higher activity change rate. The optimization process was divided into training without noise using least mean square and training with noise using maximum log likelihood. To save computing time, the parameter boundaries of training with noise were located around optimal parameter from training without noise with a narrow spread. As a result, the actual global optimal may be outside the boundary.

The predictors and components of the driver model

There are large variabilities both with respect to crash causation and driver responses in real world. Also, the driver models did not capture all the important information from the drivers (e.g., glance behaviour; however, we did remove the SHRP2 events where distraction was stated as a contributing factor) and the environment (e.g. the POV turn signal, the presence of other road users, etc.), which consequently could also be a reason of poor performance. It may also be that we missed to include some perceptual cue(s), or its derivative, that drivers use when deciding if a car warrants a braking or not.

4.2 Methodological choices

Virtual simulations are widely used in assessment of AS and ADAS functions, and there are numerous virtual simulation tools available, including OpenPass, Virtual Test Drive (VTD) and Esmini. OpenPass provides a free access framework for a reliable method of completing function effectiveness analyses (Invisiblefarm s.r.l., 2014). In Rösener et al. (2017), simulations of various scenarios were performed using OpenPass to access the safety impacts of ADAS functions from European research project AdaptIVe. VTD (Hexagon AB, 2021) is a powerful rail or road based simulation toolchain that can be use in Software in the Loop (SiL), Driver in the Loop (DiL), Vehicle in the Loop (ViL) Hardware in the Loop (HiL). Laschinsky et al. (2010) tested the influence of an Active Safety Light on the reaction of the driver using Virtual Test Drive with ViL. We had access to VTD for this thesis, but we chose not to use it because the VTD learning process (step-in effort to run a complete simulations) was much more difficult/time-consuming than Esmini's, and we also had our support (supervisor etc) only just started using VTD. Esmini is a free and open source virtual simulator and was initially developed from the Swedish collaborative research project Simulation Scenarios. It is simple to integrate it into custom applications by linking the inclusive shared library to whatever software you want to use (Emil Knabe, 2021). Volvo Cars provided scripts for integrating Esmini with Python. Another reason for selecting Esmini was that there, when we started the thesis, was an ongoing project (L3Pilot, 2021) that used Esmini for cut-in safety benefit assessment – which was a perfect fit to our thesis topic. A description of its use in L3Pilot can be found in the L3Pilot Deliverable D7.4 Impact Evaluation Results, which is currently (at the time of writing this thesis) being drafted.

Estimating derivatives from noisy signals was required in the driver models in this thesis. Kalman filter has excellent performance in dealing with signals that contains Gaussian noise and was therefore chosen for this part. Shaowei & Shanming (2012) used a Kalman filter with adaptive noise variance to estimate motor velocity, with results that were very close to the actual values. Moving average filters are also commonly used to estimate derivatives from noisy signals, and they are conceptually and practically simple to understand and implement. Kalman Filter is a more accurate and smoothing prediction algorithm comparing to the moving average filter, because it is adaptive and it takes estimation errors from different sources (and processes) into account, and tries to adjust the predicted values based on what it learned in the previous stage (CQG Integrated Client, 2021). The estimation results from an average moving filter will lag behind the true state. It will be more accurate if a larger time interval is used, but the lagging will be more severe.

In terms of model parameter fitting, the models in this thesis are complex, with a large number of parameters, which means using random search and grid search would be inefficient (Liashchynskyi & Liashchynskyi, 2019). Furthermore, because it is not a differentiable problem, any algorithm involving gradient descent was out of the

question. We used PSO as the optimization technique for fitting model parameters. There are other Evolutionary Algorithms that are similar, such as Genetic Algorithm (GA) and Differential Evolution (DE). DE and PSO are better suited to continuous optimization, whereas GA is more suitable for discrete optimization (Kachitvichyanukul, 2012). In parameter fitting of the accumulation driver model, DE and PSO are preferable to GA because the parameters can be set to any value within the boundary. It was also mentioned in Kachitvichyanukul (2012) that, comparing to DE , the global optimal of PSO in each iteration has a dominant influence over the whole swarm, which enables solution improvement with shorter time (than DE). However, diversification of DE is better than PSO because the best solution in the population has no influence on the other solutions in the population. In Zgonnikov et al. (2020), an accumulation driver model was developed for predicting whether the drivers will make a left turn across path of an oncoming car. The model was fitted into data in terms of probability of turn decisions and the response time for the "turn" decisions. DE was chosen using cost function of weighted least sum score. While in Svärd et al. (2020) and this thesis, the calculation of cost (maximum log likelihood) of each parameter set requires a large number of repeating simulations to generate a 2D distribution of break onset timing and jerk, which means a high computing time. As a result, PSO may be a better solution than DE.

4.3 Limitations and Future work

The SHRP2 dataset that were available to us contained 209 cut-in events with forward facing video, but after we applied the inclusion and exclusion criteria only 18 events remained (Section 2.1). Removing 191 (91.3%) events and only having 18 events "to work with" was naturally a major limitation. However, we believe that our focus on the methodological aspects of the modelling, and the design of relevant predictors still provided a good thesis and learning opportunities, and results that can be a stepping stone for future research. One solution to improve the data quality is either use a different data extraction tool or improve video annotation tool, or a different dataset, if available.

Initially, there was supposed to be four different driver models, but due to limited time, one driver (Model 4) was excluded in this study. Model 4 (proposed, not implemented) is more based on human peripheral vision and how driver utilize peripheral vision to perform different driving task. This includes object movement, road signs, monitor traffic, stay within the lane etc. (Edmund Hunter, n.d.). The POV will mostly be inside the EGO peripheral vision during cut-ins but if the POV is outside "center of vision", the driver may react slower to cut-ins. First the EGO driver needs to identify the object with his/her the peripheral vision, then move the eyes to it, then make a decision based on the situation, and, finally initiate a brake response, if needed. All this together may add to the brake respond "delay". However, this is likely to not be an issue if the EGO driver is already looking at the POV at the start of cut-in event. Consequently, glance behavior data for each event is needed in the modelling to enable the consideration of peripheral versus foveal vision in the model. Specifically, Model 4 utilize human peripheral vision in traffic as a constraint. Studies show that peripheral vision will change depending on speed, and that may have in impact on how peripheral vision should be included in the model (Shbeeb, 2016). Model 4 could potentially have increased the performance of the model, but was never implemented and fitted to the data. The Wolfe et al. (2017) report demonstrated this peripheral vision in traffic with live camera, to get a clearer picture how this looks in real traffic with center of vision

(Figure 3 on p. 321 in Wolfe et al. (2017)). When the driver is changing their focus area (center of vision), everything outside the focus area becomes blurry. In the picture (Figure 3 p. 321 in Wolfe et al. (2017)), a red circle is where driver is currently looking. When the driver is shifting their center of vision from b to c and c to d, everything outside the red circle is blurry. This is an interesting phenomenon to investigate for future cut-in driver models, as it may substantially affect the perception and response in cut-in situations.

We started the work using an already existing dataset, that late in the thesis work was found to have errors in the POV lateral position. Before we found this and addressed it (through semi-manual correction) we conducted several analyses on the data that we did not have time to redo on the new dataset. For example, on the original dataset we performed random selection of event and K-Fold cross-validation to analyse the sensitivity of event selection and data variability. K-Fold cross-validation is a popular method in machine learning world to estimate the performance of models and selection of models (Jung, 2018). Such analysis requires a lot of computing time and therefor was left for future investigation for the new (corrected) dataset. The initial plan was also to use this training process to reduce number of trained parameters. The remaining 18 events was divided into two different set, 12 events for training and 6 for test. This training data is extremely small for such complex driver model with 8 free parameters. The size of training data might not be large enough to optimize the parameters using PSO. As for the future, increasing the training dataset, reducing complexity of the model and reduce simulation time will allow more time for trial and error, improve the driver model performance. Because optimisation with noise required a high computing time, it was only done once with relatively low interactions and a narrow parameter boundary. The true optimal value could lay outside of the boundary. Finding a better way to define parameter boundaries could aid in the resolution of this issue. Another option is to reduce the model's complexity. When the model has a small number of parameters, fewer interactions and less computation time are required.

The complexity and limited time available for this thesis were major factors in how what we pursued and what we could complete. For example, driver off-road glance behaviour was not considered in this thesis, although it is an important part. Driver distraction is a normal behaviour in traffic and can greatly deteriorates driving performance (Donmez et al., 2010). Future studies should investigate the role of the driver's peripheral vison versus fovia vision on the cut-in vehicle. As mentioned before, the discontinuity of $P(t)$ at POV-in-lane timing, caused by the changing of calculation equations, should be studied in future work, with the aim to create a continues accumulation function. Finally, this work is one step in the direction of driver response models for cut-in scenarios. With further development we hope that it can be used as part of virtual safety benefit assessment of active safety systems and possibly for vehicles with higher levels of automation.

5 Conclusion

This thesis extended an existing rear-end accumulation driver model to a cut-in driver model to predict the braking of the driver. This study showed it is possible to use the video annotation tool to extract necessary information from naturalistic driving data and later reconstruct near-crash events in virtual simulation. Three model proposals with different perceptual input calculations were introduced and implemented in virtual simulation. The model's parameter was optimized with the stochastic optimization method PSO, to fit the parameters to real-world naturalistic near-crash data. The optimization process was divided into two separate parts, one without noise and second one with noise to save more computing time. Model 1 was only activated after POV-in-lane and it had the worst performance (late response), which indicated that in real world, the driver usually response before the POV reached the lane mark. The best performing model (Model 3) were selected for training with noise and had more parameters (8 in total) compared to rear-end driver model from previous work. This indicate that sometimes it is necessary to increase the model complexity in order to capture more perceptual cues from drivers. The validation method of the models was based on previous work on rear-end driver model.

The Model 3 had a better performance than Model 1 and 2 but it still not good enough. The models did not capture all the necessary mechanisms, such as glance behaviour or distraction was excluded in this study. The model needs further improvement, both by reducing the complexity of the model (reduce computing time) and adding additional relevant parameters that can capture more information about the driver (improve accuracy). However, Model 3 did perform well on brake onset timing but showed weaker jerk compared to real drivers in some of the simulations. With further development, the driver model could be used in virtual simulations to do safety assessment of active safety or other vehicle automation functions. A future validated driver model could mimic the possible reactions from a driver in a cut-in situation, and, consequently being used to generate baseline events and as part of warning strategies in cut-in conflicts. Including some variability in the parameters (including noise) can make the situation is a little bit different (but capturing within and between driver variabilities), making the assessment results more robust.

6 References

Almeida, B. S. G. de, & Leite, V. C. (2021). *Particle Swarm Optimization: A Powerful Technique for Solving Engineering Problems*. 2019-12-03. https://www.intechopen.com/books/swarm-intelligence-recent-advances-new-perspectives-and-applications/particle-swarm-optimization-a-powerful-technique-for-solving-engineering-problems

Bärgman, J. (2019). *Signal processing assignment from Vehicle and Traffic Safety*. Chalmers University of Technology.

Benderius, O. (2012). Driver modeling: data collection, model analysis, and optimization. *Thesis for Licentiate of Engineering, 2012:11*, 58. http://publications.lib.chalmers.se/records/fulltext/157634.pdf%0Ahttps://trid.trb.org/view/1367670

Chovan, J. D., Tijerina, L., Alexander, G., & Hendricks, D. L. (1994). Examination of Lane Change Crashes and Potential IVHS Countermeasures. *Report No. DOT HS 808 071, U.S. Department of Transportation, March*, 50.

CQG Integrated Client. (2021). *Basic Studies - Kalman Filter*. CQG Integrated Client.

Din, A. H. S. El, Takkoush, M., Pettersson, N., & ... (2020). *Variables extraction and trajectory reconstruction for modelling driver behaviour*. https://odr.chalmers.se/handle/20.500.12380/300751

Donmez, B., Boyle, L. N., & Lee, J. D. (2010). Differences in off-road glances: Effects on young drivers' performance. *Journal of Transportation Engineering*, *136*(5), 403–409. https://doi.org/10.1061/(ASCE)TE.1943-5436.0000068

Edmund Hunter. (n.d.). *Module 3: Topics 1-3 Vision and Driving*. 2016 IEEE 19th International Conference on Intelligent Transportation Systems (ITSC). https://slideplayer.com/slide/10872053/

Emil Knabe. (2021). *Environment Simulator Minimalistic (esmini)*. 2021. https://github.com/esmini

Gordon, T., & Srinivasan, K. (2014). Modeling human lane keeping control in highway driving with validation by naturalistic data. *Conference Proceedings - IEEE International Conference on Systems, Man and Cybernetics*, *2014-Janua*(January), 2507–2512. https://doi.org/10.1109/smc.2014.6974303

Helmer, T., Wang, L., Kompass, K., & Kates, R. (2015). Safety Performance Assessment of Assisted and Automated Driving by Virtual Experiments: Stochastic Microscopic Traffic Simulation as Knowledge Synthesis. *2015 IEEE 18th International Conference on Intelligent Transportation Systems*, 2019–2023. https://doi.org/10.1109/ITSC.2015.327

Hexagon AB. (2021). *Virtual Test Drive*. 2021. https://www.mscsoftware.com/product/virtual-test-drive

Invisiblefarm s.r.l. (2021). *OpenPass for open system of controlled access*. 2014. http://www.openpass.it/

Jung, Y. (2018). Multiple predicting K-fold cross-validation for model selection. *Journal of Nonparametric Statistics*, *30*(1), 197–215. https://doi.org/10.1080/10485252.2017.1404598

Kachitvichyanukul, V. (2012). Comparison of Three Evolutionary Algorithms: GA, PSO, and DE. *Industrial Engineering and Management Systems*, *11*, 215–223.

L3Pilot. (2021). *L3Pilot*. L3Pilot.

Laschinsky, Y., von Neumann-Cosel, K., Gonter, M., Wegwerth, C., Dubitzky, R., & Knoll, A. (2010). Evaluation of an Active Safety Light using Virtual Test Drive within Vehicle in the Loop. *2010 IEEE International Conference on Industrial Technology*, 1112–1119. https://doi.org/10.1109/ICIT.2010.5472583

Liashchynskyi, P., & Liashchynskyi, P. (2019). *Grid Search, Random Search, Genetic Algorithm: A Big Comparison for NAS*.
Markkula, G. (2014). Modeling driver control behavior in both routine and near-accident driving. *Proceedings of the Human Factors and Ergonomics Society*, *2014-Janua*, 879–883. https://doi.org/10.1177/1541931214581185
Markkula, G., Benderius, O., Wolff, K., & Wahde, M. (2012). A review of near-collision driver behavior models. *Human Factors*, *54*(6), 1117–1143. https://doi.org/10.1177/0018720812448474
Page, Y., Fahrenkrog, F., Fiorentino, A., Gwehenberger, J., Helmer, T., Lindman, M., Camp, O., Rooij, L. V, Puch, S., Fränzle, M., Sander, U., & Wimmer, P. (2015). *A comprehensive and harmonized method for assessing the effectiveness of advanced driver assistance systems by virtual simulation: The P.E.A.R.S.*
QUADRAE. (2021). *QUADRAE*. 2021-03-31. https://www.saferresearch.com/projects/quadrae
Rösener, C., Sauerbier, J., Zlocki, A., Fahrenkrog, F., Wang, L., Varhelyi, A., Gelder, E., Breunig, S., Tango, F., & Lanati, J. (2017). *A Comprehensive Evaluation Approach for Highly Automated Driving*.
Shams El Din, A. H. (2020a). *Statistical modelling of critical cut-ins for the evaluation of autonomous vehicles and advanced driver assistance systems*. https://hdl.handle.net/20.500.12380/301054
Shams El Din, A. H. (2020b). *Statistical modelling of critical cut-ins for the evaluation of autonomous vehicles and advanced driver assistance systems*.
Shaowei, W., & Shanming, W. (2012). Velocity and acceleration computations by single-dimensional Kalman filter with adaptive noise variance. *Przeglad Elektrotechniczny*, *88*(2), 283–287.
Shbeeb, D. L. (2016). *Human component and vehicle in transportation*. 2016-01-30. https://www.slideshare.net/hronaldo10/driver-vehicle-transportation-engineering-drlina-shbeeb?fbclid=IwAR3uQimT1K00a65CNugQtPEtTr9wDLHmiN3QUlOMQtp3z4XQSrFaSLJchZc
Svärd, M., Markkula, G., Bärgman, J., & Victor, T. (2020). *Computational modeling of driver pre-crash brake response, with and without off-road glances: Parameterization using real-world crashes and near-crashes*. https://doi.org/10.31234/osf.io/6nkgv
Svärd, M., Markkula, G., Engström, J., Granum, F., & Bärgman, J. (2017). A quantitative driver model of pre-crash brake onset and control. *Proceedings of the Human Factors and Ergonomics Society Annual Meeting*, *61*(1), 339–343. https://doi.org/10.1177/1541931213601565
Virginia Tech Transportation Institute. (n.d.). *DATA REDUCTION*. 2021. https://www.vtti.vt.edu/facilities/data-reduction.html
Virginia Tech Transportation Institute. (2021). *InSight Data Access Website SHRP2 Naturalistic Driving Study*. 2020. https://insight.shrp2nds.us/
Wolfe, B., Dobres, J., Rosenholtz, R., & Reimer, B. (2017). More than the Useful Field: Considering peripheral vision in driving. *Applied Ergonomics*, *65*, 316–325. https://doi.org/10.1016/j.apergo.2017.07.009
Zgonnikov, A., Abbink, D., & Markkula, G. (2020). *Should I stay or should I go? Evidence accumulation drives decision making in human drivers*. https://doi.org/10.31234/osf.io/p8dxn

Appendix

Result of Model 3 – training without noise 1st run – training set

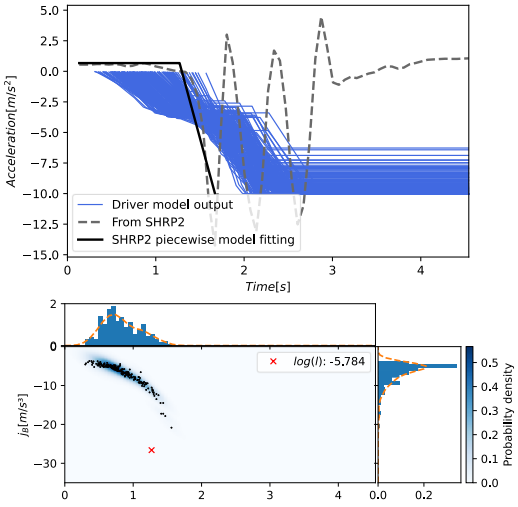

Figure 36 Event1

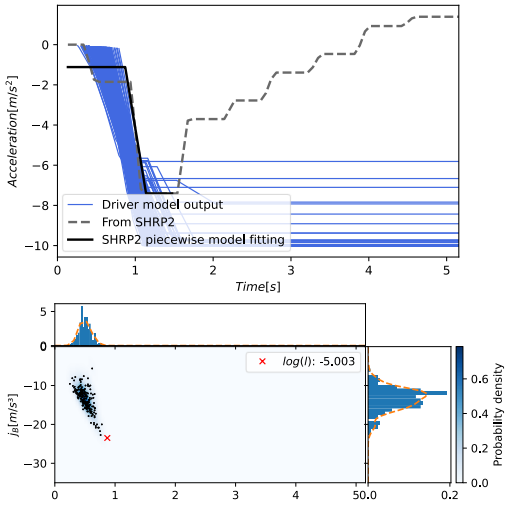

Figure 37 Event2

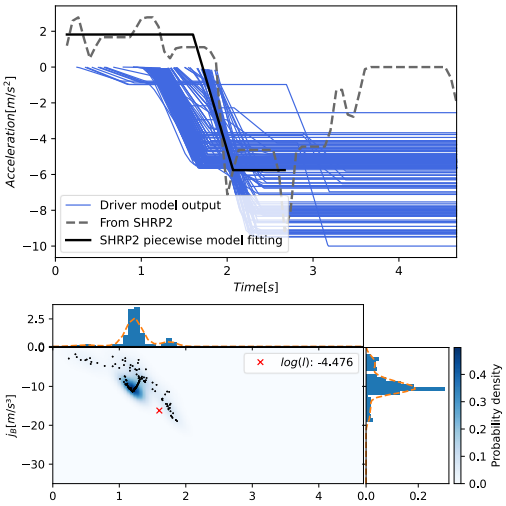

Figure 38 Event3

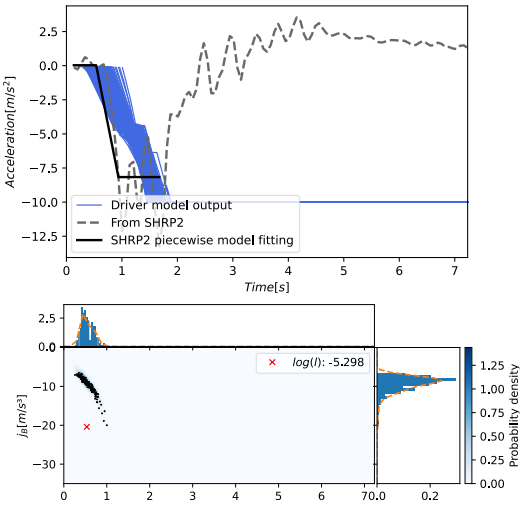

Figure 39 Event4

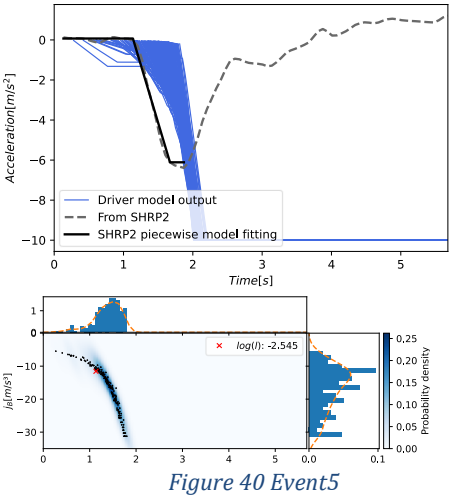

Figure 40 Event5

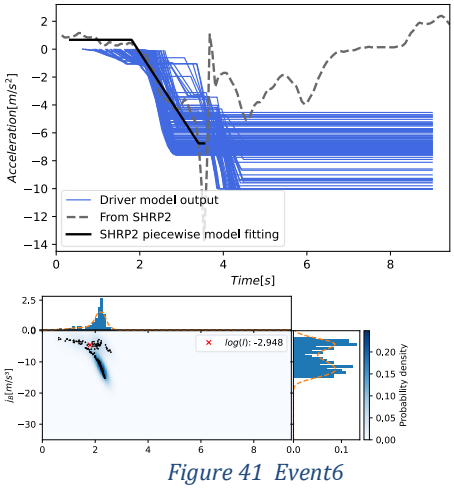

Figure 41 Event6

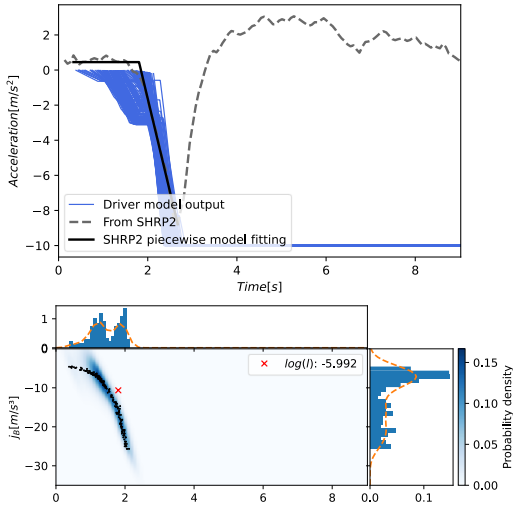

Figure 42 Event7

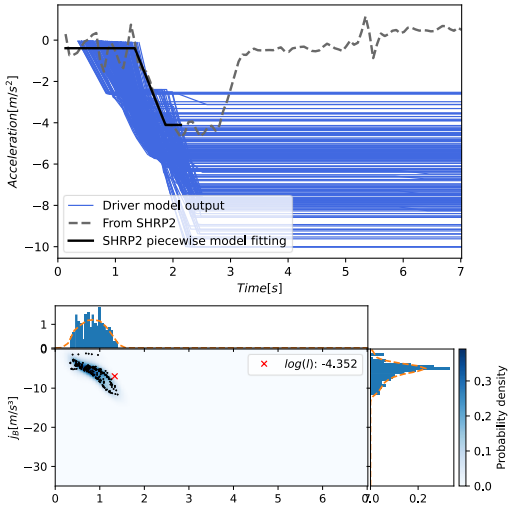

Figure 43 Event8

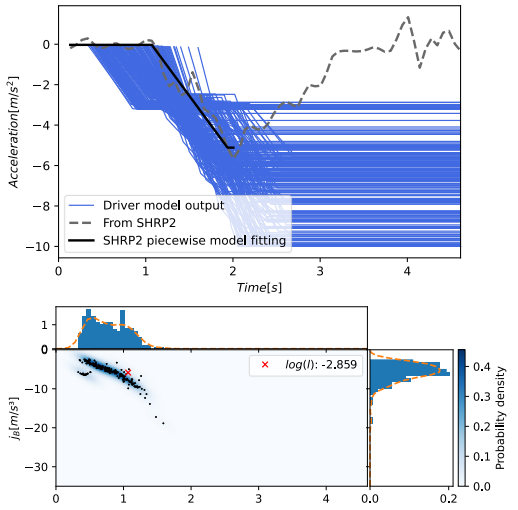

Figure 44 Event9

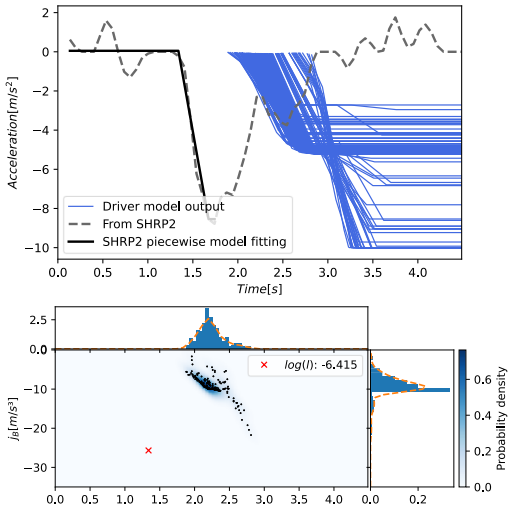

Figure 45 Event10

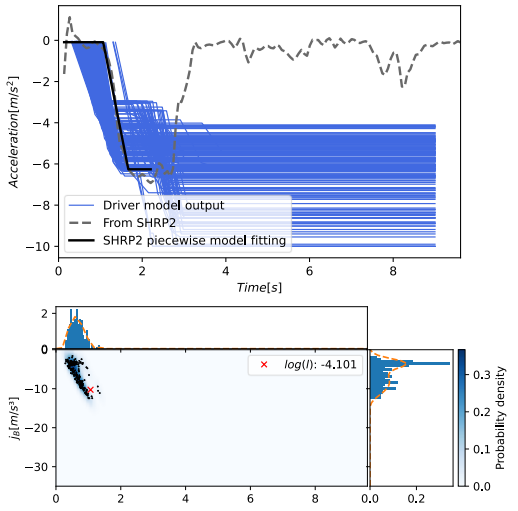

Figure 46 Event11

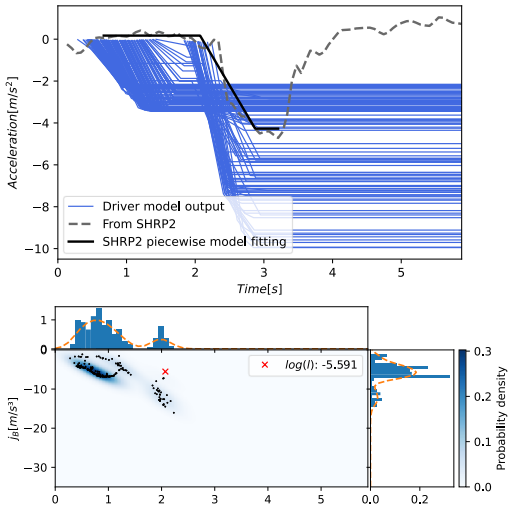

Figure 47 Event12

Result of Model 3 – training without noise 1st run – test set

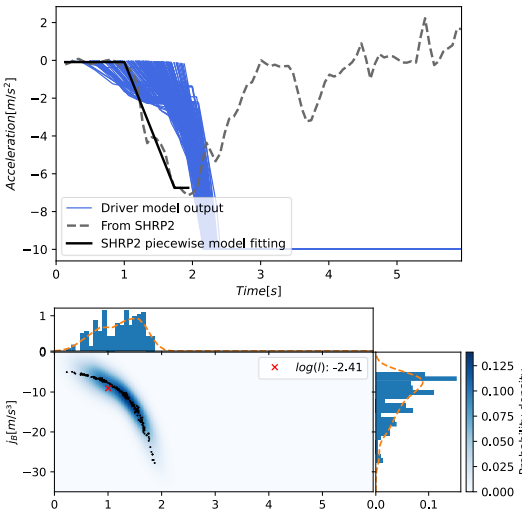

Figure 48 Event13

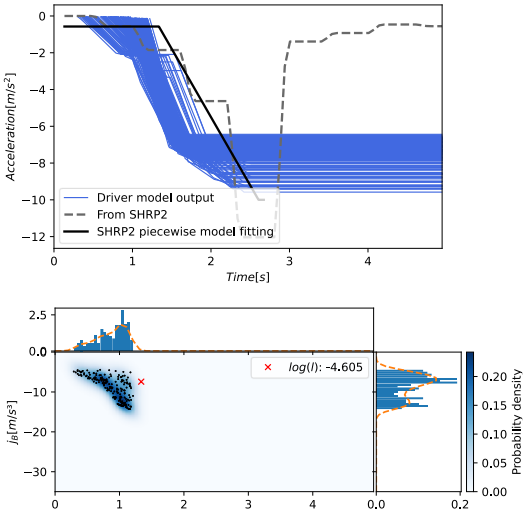

Figure 49 Event14

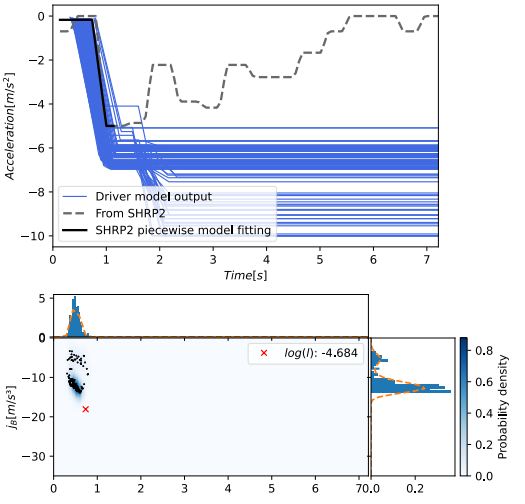

Figure 50 Event15

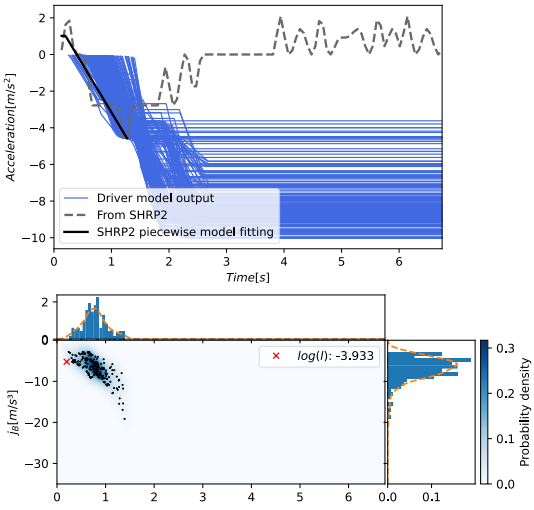

Figure 51 Event16

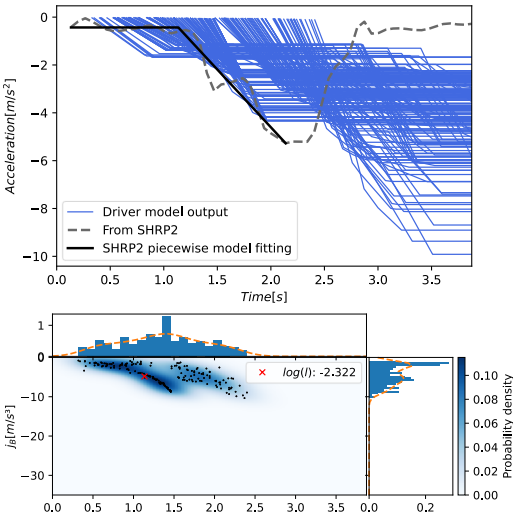

Figure 52 Event17

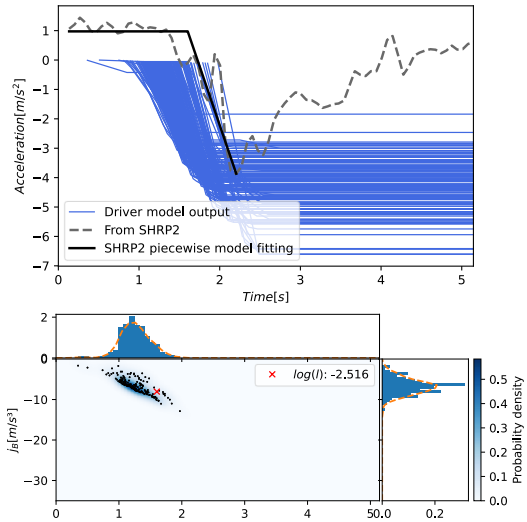

Figure 53 Event18

Result of Model 3 – training with noise – training set

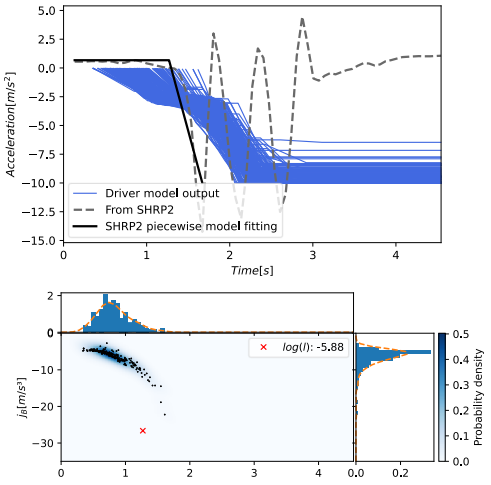

Figure 54 Event1

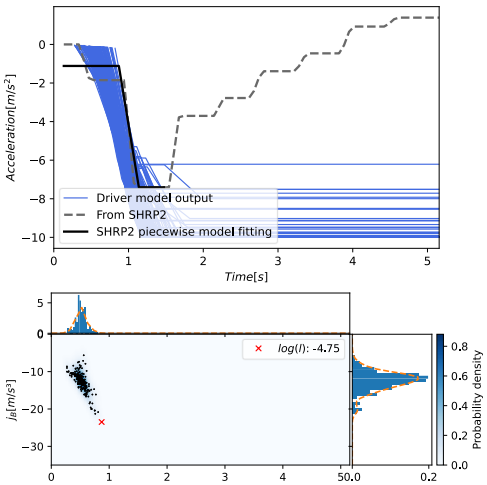

Figure 55 Event2

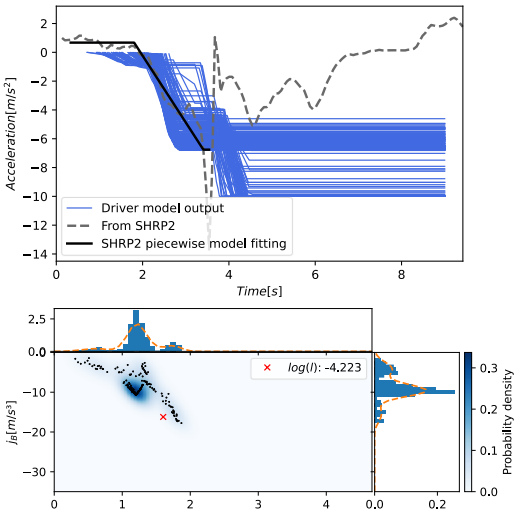

Figure 56 Event3

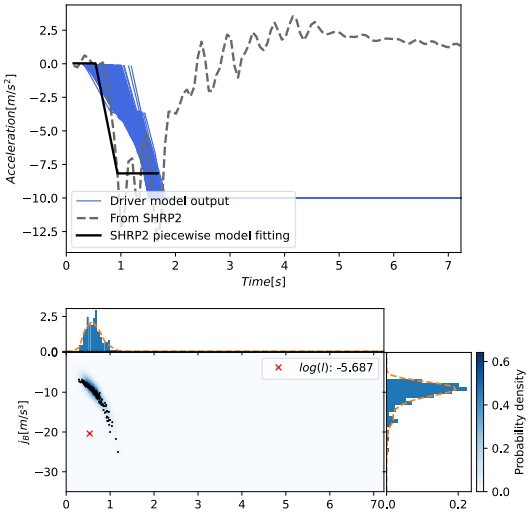

Figure 57 Event4

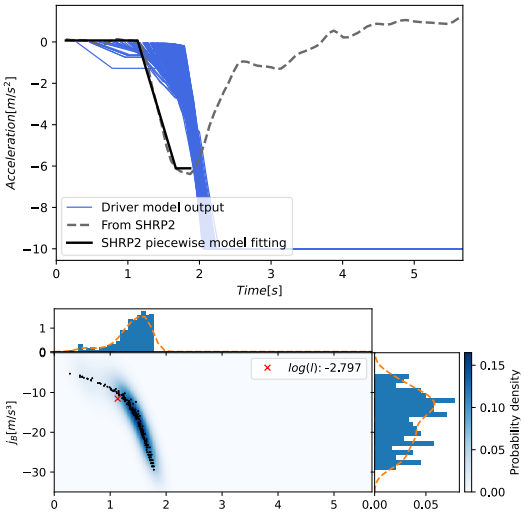

Figure 58 Event5

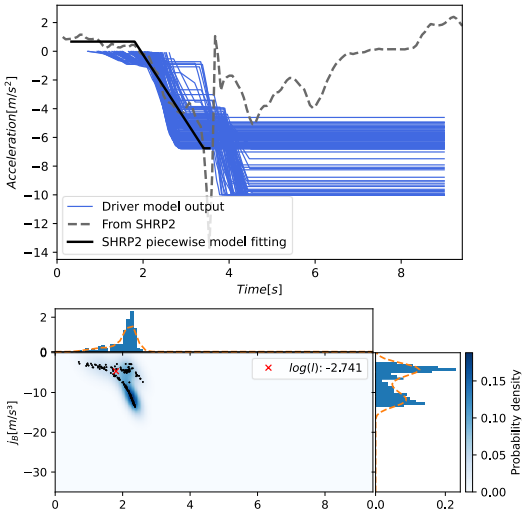

Figure 59 Event6

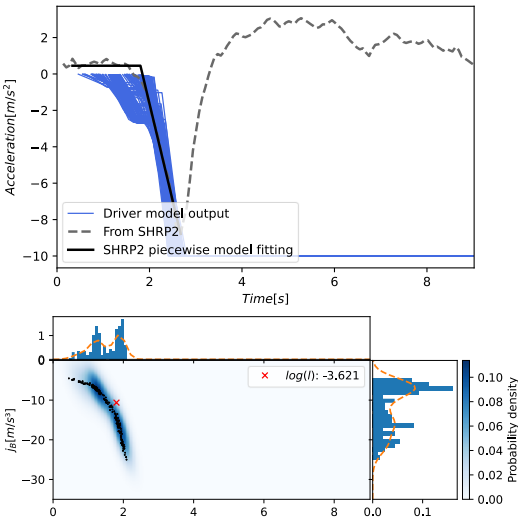

Figure 60 Event7

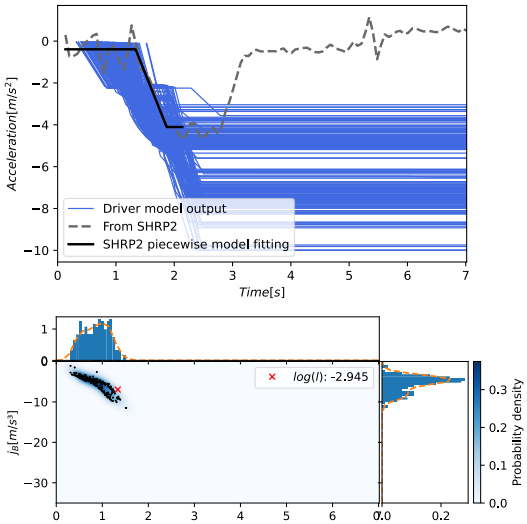

Figure 61 Event8

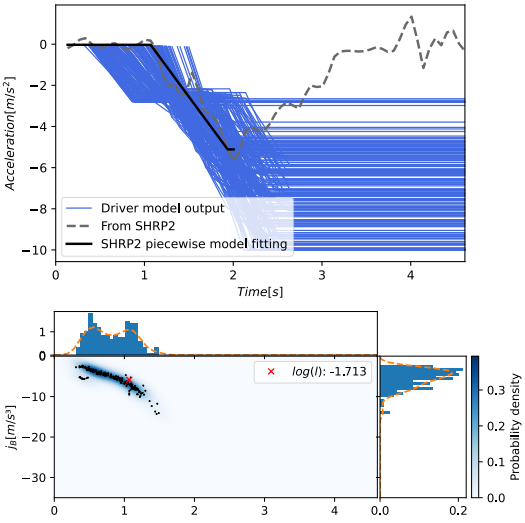

Figure 62 Event9

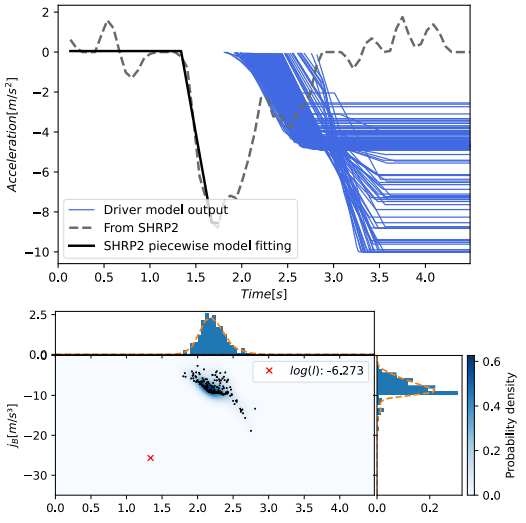

Figure 63 Event10

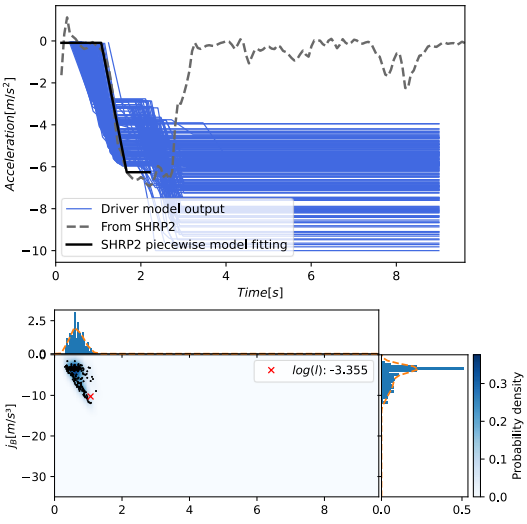

Figure 64 Event11

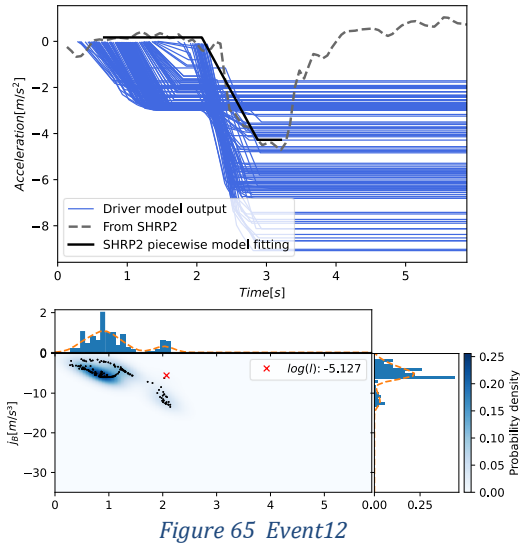

Figure 65 Event12

Result of Model 3 – training with noise – test set

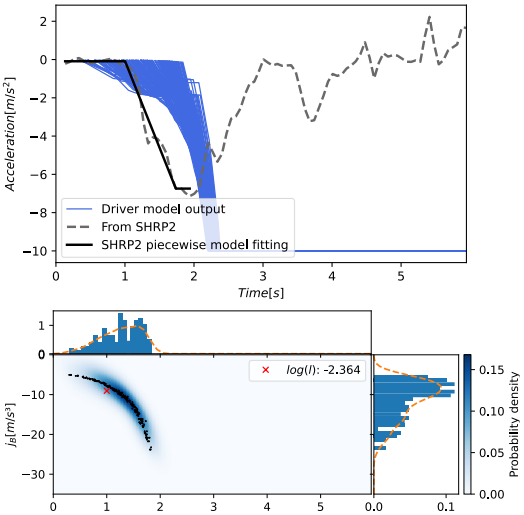

Figure 66 Event13

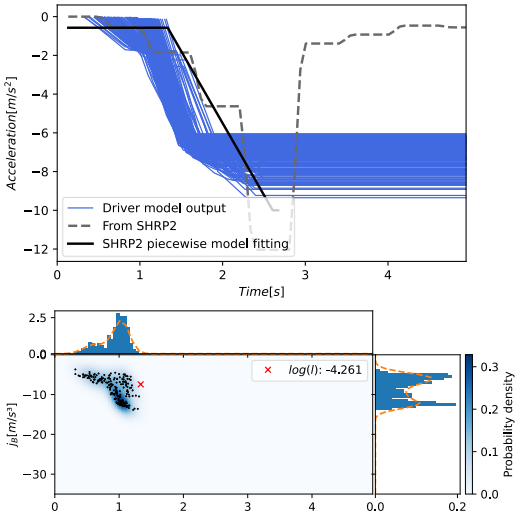

Figure 67 Event14

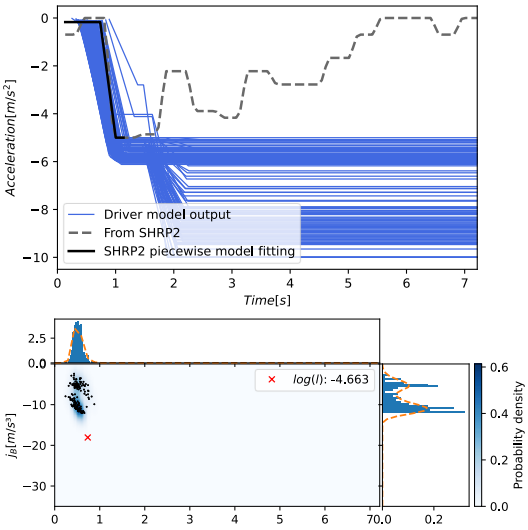

Figure 68 Event15

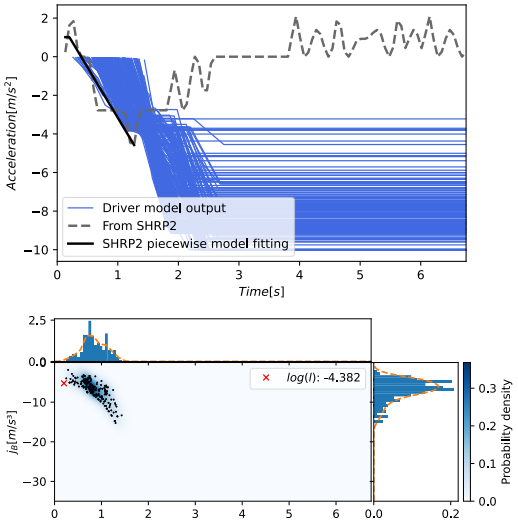

Figure 69 Event16

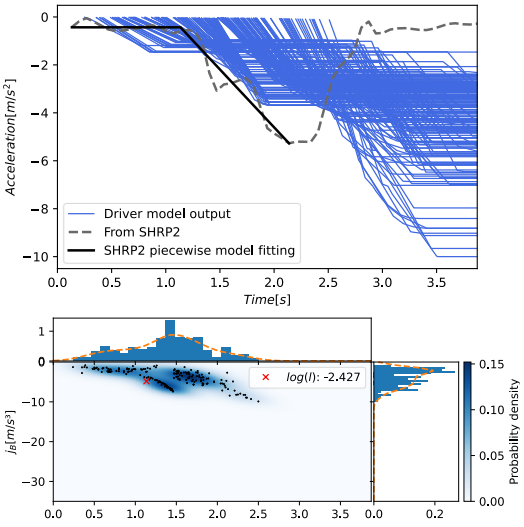

Figure 70 Event17

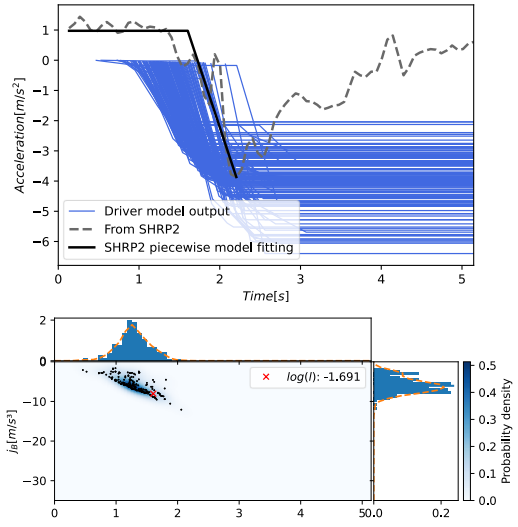

Figure 71 Event18

DEPARTMENT OF MECHANICS AND
MARITIME SCIENCE CHALMERS
UNIVERSITY OF TECHNOLOGY
Gothenburg, Sweden 2021
www.chalmers.se

CHALMERS
UNIVERSITY OF TECHNOLOGY